doi.org/10.36721/PJPS.2026.39.4.REG.14438.1

Computational exploration of *Withania coagulans*-derived natural inhibitors targeting HMG-CoA reductase: A pharmacokinetic, docking and molecular dynamics study for cholesterol regulation in *Mus musculus*

Muhammad Bilal Azmi[1]*, Fearoz Khan[2,3], Uzma Asif[4], Fatimah Hoda[5], Sheikh Arslan Sehgal[6], Shamim A Qureshi[2] and Syed Danish Haseen Ahmed[1]

[1]Computational Biochemistry Research Laboratory, Department of Biochemistry, Dow Medical College, Dow University of Health Sciences, Karachi, Pakistan
[2]Department of Biochemistry, University of Karachi, Karachi, Pakistan
[3]Department of Biochemistry, Swat Medical College, Saidu Sharif, Swat, Pakistan
[4]Department of Biochemistry, Medicine Program, Batterjee Medical College, Jeddah, Saudi Arabia
[5]Dow Medical College, Dow University of Health Sciences, Karachi, Pakistan
[6]Department of Genomics and Bioinformatics, Cholistan University of Veterinary and Animal Sciences, Bahawalpur, Pakistan

Abstract: **Background**: Hypercholesterolemia is a major modifiable risk factor for cardiovascular disease, largely driven by excessive activity of 3-hydroxy-3-methylglutaryl-CoA reductase (Hmgcr), the rate-limiting enzyme in cholesterol biosynthesis. Although statins are effective inhibitors of this enzyme, their long-term use is often limited by their adverse effects. This has encouraged the search for safer, plant-derived alternatives. *Withania coagulans*, a medicinal plant rich in withanolides, has demonstrated lipid-lowering potential; however, its molecular interactions with Hmgcr remain insufficiently explored. **Objectives**: This study aimed to identify and characterize bioactive compounds from *Withania coagulans* as potential natural inhibitors of Hmgcr in *Mus musculus*, using an integrated *in silico* strategy. **Methods**: A validated three-dimensional model of *Mus musculus* Hmgcr was generated using homology modeling. Twenty bioactive compounds from *Withania coagulans*, along with standard statins, were screened using molecular docking and ADMET profiling, following Lipinski's rule of five. High-ranking complexes were further explored using MM/PBSA and MM/GBSA binding-free energy calculations. Molecular dynamics simulations (100 ns) were performed for top-ranked selected ligand–protein complexes to assess their structural stability and interaction persistence under physiologically relevant conditions. **Results**: Several *Withania coagulans* compounds demonstrated strong binding affinities toward the Hmgcr active site, in some cases comparable to or exceeding those of standard statins. The key interactions involved conserved catalytic residues, such as Tyr516, Met533, Ile535, Ile761, Pro812 and Gln813. Molecular dynamics analyses revealed stable complexes with low RMSD fluctuations and minimal active site flexibility, confirming sustained ligand binding. ADMET predictions suggested favorable oral absorption and acceptable drug-like properties for the leading compounds. **Conclusion**: This study highlights *Withania coagulans* as a promising source of natural Hmgcr inhibitors. The identified compounds exhibited stable binding, favorable pharmacokinetic profiles, and mechanistic similarity to established statins, supporting their potential for further experimental validation as cholesterol-lowering agents.

Keywords: Hmgcr; Molecular docking; Molecular dynamics; *Mus musculus*; *Withania coagulans*

Submitted on 08-04-2025 – Revised on 08-09-2025 – Accepted on 15-09-2025

INTRODUCTION

Hypercholesterolemia, a pathophysiological condition characterized by elevated LDL-C levels, is a significant modifiable risk factor for atherosclerosis and its symptoms often appear later in disease progression (Ahangari *et al*., 2018; Prasad and Mishra, 2022). According to World Health Organization (WHO) statistics, approximately 39% of the global adult population has elevated total cholesterol levels (Ahangari *et al*., 2018). A 2022 study reported that high levels of low-density lipoprotein cholesterol (LDL-C) were linked to 4.4 million deaths worldwide in 2019, accounting for 12.6% of all deaths attributable to risk factors (Zheng *et al*., 2022).

Atherosclerosis is a multifactorial disease characterized by endothelial activation, lipid accumulation, fibrous tissue formation and vascular calcification, which ultimately leads to vessel narrowing and chronic inflammation (Jebari-Benslaiman *et al*., 2022). As a major contributor to cardiovascular disease (CVD), atheromatous plaque progression not only disrupts normal blood flow but also increases the risk of life-threatening cardiovascular complications, making it a leading cause

**Corresponding author:* e-mail: bilal.azmi@duhs.edu.pk

of mortality worldwide (Bjorkegren and Lusis, 2022). In hypercholesterolemia, research has demonstrated accelerated production of reactive oxygen species (ROS) and various cytokines, which in turn increase the expression and release of cell adhesion molecules, ultimately leading to the formation of atheromatous plaques (Prasad and Mishra, 2022). This pathological process begins with endothelial activation, initiating a cascade of events that includes narrowing of vessels and initiation of inflammatory pathways, ultimately resulting in atheroma formation (Jebari-Benslaiman *et al*., 2022; Prasad and Mishra, 2022). ROS further amplify the production of growth factors, transforming growth factors, and cell adhesion molecules. Moreover, ROS promotes the oxidation of low-density lipoprotein cholesterol (LDL-C), initially generating minimally modified LDL-C (MM-LDL), which is subsequently oxidized into fully oxidized LDL (ox-LDL). MM-LDL induces the production of monocyte chemoattractant protein-1 (MCP-1) and monocyte colony-stimulating factor from endothelial cells, whereas ox-LDL facilitates foam cell formation and monocyte migration into the subendothelial space (Prasad and Mishra, 2022). Consequently, hypercholesterolemia plays a critical role in the pathogenesis of atherosclerosis through the generation of these biomolecules (Jebari-Benslaiman *et al*., 2022; Prasad and Mishra, 2022).

The cholesterol synthesis pathway involves the conversion of HMG-CoA to mevalonate, which is the rate-limiting step in cholesterol synthesis. Statins lower cholesterol levels by directly inhibiting HMG-CoA reductase, the enzyme responsible for this step. The subsequent decrease in intracellular cholesterol activates sterol regulatory element-binding protein (SREBP)-2, which is the body's compensatory response. This activation increases the expression of genes such as HMG-CoA reductase (HMGCR) and the LDL-C receptor (LDLR), aiming to restore cholesterol balance by enhancing cholesterol synthesis and uptake (Chen *et al*., 2019). Statins, which act through similar mechanisms, are widely used to lower cholesterol levels; however, prolonged use in patients with other comorbidities can increase susceptibility to side effects, such as statin-associated muscle symptoms (SAMS) (Dicken *et al*., 2022). Some statins may also be diabetogenic and cause elevated liver enzyme levels. With the increasing recognition of the side effects of synthetic medications, researchers have shifted their focus to developing plant-based alternatives that are natural, cost-effective, and safer, with fewer adverse effects (Carmena and Betteridge, 2019; Pinal-Fernandez *et al*., 2018). The use of medicinal plants to treat various diseases is an age-old concept that has been practiced for centuries. Many plants are valued for their notable antioxidant, antithrombotic, anti-inflammatory, antiatherogenic, and cardioprotective properties (Nwozo *et al*., 2023).

Withania coagulans, a medicinal plant with significant therapeutic potential, has garnered attention for its broad-spectrum pharmacological properties (Sinoriya *et al*., 2024). Various studies have demonstrated its efficacy in managing and treating multiple conditions, including diabetes, bacterial and microbial infections, liver disorders, hyperlipidemia, oxidative stress, cancer, depression, and inflammation (Tahir *et al*., 2024). In addition, the plant exhibits notable antioxidant, immunosuppressive, and anti-inflammatory activities (Sinoriya *et al*., 2024). The fruit of *Withania coagulans* is rich in bioactive compounds, including esterases, free amino acids, fatty oils, essential oils, and, most importantly, withanolides (Khan *et al*., 2021). Withanolides, a major class of phytochemicals in this species, are polyhydroxy C28 steroidal lactones, which are secondary metabolites (Khan *et al*., 2021; Sinoriya *et al*., 2024). Several distinct withanolides have been identified in *Withania coagulans,* including coagulin F, coagulanolide, withacoagulin, and coagulin G (Khan *et al*., 2021). These withanolides are believed to play a key role in the pharmacological effects of these plants, contributing to their therapeutic potential.

In 2023, a preliminary study computationally characterized a few bioactive compounds from *Withania coagulans* as potential inhibitors of HMG-CoA reductase, highlighting their role in regulating lipid metabolism (Azmi *et al*., 2023). Expanding on this, we investigated the lipid-lowering potential of these natural products by examining their effects on cholesterol-regulating gene in *Mus musculus*. Given the absence of a complete structural model, computational techniques were employed to predict the 3D structure of HMG-CoA reductase, which is a key enzyme in cholesterol homeostasis. Using molecular docking and molecular dynamics (MD) simulations, we analyzed the binding interactions between the enzyme and *Withania coagulans*-derived compounds. Additionally, we evaluated their drug-likeness, ADMET properties, and toxicity profiles, providing valuable insights into their therapeutic potential as cholesterol-lowering agents.

MATERIALS AND METHODS

Sequence retrieval, alignment, structural modeling and ligand preparation for Hmgcr protein targeting

To investigate the *Hmgcr* gene in *Mus musculus*, its sequence was retrieved from the UniProt database (https://www.uniprot.org/) and verified against NCBI records and the relevant literature (Sayers *et al*., 2021). The FASTA sequence obtained from NCBI was used as the basis for the sequence analysis. The physicochemical properties of HMG-CoA reductase were analyzed using the Protein Identification and Analysis Tools on the Expasy Server (https://web.expasy.org/protparam/) to better understand how its structural features might

influence ligand interactions and protein stability. The molecular weight and theoretical isoelectric point (*pI*) were evaluated to infer solubility and charge distribution, which can affect electrostatic interactions with ligands. The instability index was calculated to assess protein stability under physiological conditions, which is relevant for predicting the duration of functional enzyme activity in a cellular environment. Protein BLAST (Basic Local Alignment Search Tool) was then used to assess sequence homology, with the *M. musculus* protein serving as a query to identify template structures from the Protein Data Bank (PDB) for subsequent modeling.

Because no experimentally determined crystal structure of *Mus musculus* HMG-CoA reductase was available in the Protein Data Bank, we used homology modeling to predict its three-dimensional structure. Initially, high-identity templates were identified through BLAST searches and used in MODELLER to build several candidate models (Webb and Sali, 2021). To ensure structural reliability, we evaluated the models using several standard quality metrics. Ramachandran plots were generated to assess stereochemical properties, verifying that the majority of residues were in the most favored regions. In addition, the quality factor scores and overall model energy profiles were reviewed to detect any unfavorable geometry. However, these models showed relatively low-quality factor scores and several residues in the disallowed regions of the Ramachandran plot, indicating suboptimal stereochemistry. To address these limitations and improve structural accuracy, we employed SWISS-MODEL as an alternative homology modeling strategy. This automated platform uses high-quality template selection, optimized alignment, and built-in energy minimization protocols to generate refined protein structures. The SWISS-MODEL-derived structure showed a markedly improved quality factor, with no residues in the disallowed regions and better overall stereochemical properties. This validated homology model was then used as the structural basis for downstream molecular docking, focusing on the known consensus binding residues and druggable sites, ensuring reliable and biologically meaningful protein–ligand interaction predictions (Webb and Sali, 2021; Waterhouse *et al.*, 2018). Structural analyses, including interactive visualization via UCSF Chimera and energy minimization using Swiss-PdbViewer (DeepView), were performed to enhance model stability (Guex *et al*., 2009; Pettersen *et al*., 2021). Model validation was performed using PROCHECK for stereochemical analysis, ERRAT for structural evaluation, ProsaWeb (https://prosa.services.came.sbg.ac.at/prosa.php) for reliability scoring, and Ramachandran plots to assess dihedral angles. Further structural integrity checks were conducted using the SAVES (https://saves.mbi.ucla.edu/) server and PDBsum to ensure robust model validation and a detailed secondary structure assessment.

For ligand preparation, 3D structures of lipid-lowering agents as potential inhibitors of Hmgcr were retrieved from PubChem (https://pubchem.ncbi.nlm.nih.gov/) (Kim *et al*., 2021). Additionally, a curated library of bioactive compounds from *Withania coagulans* was compiled from extensive literature, with structures sourced from PubChem in the SDF format and converted to the PDB format via Open Babel to ensure compatibility (https://www.cheminfo.org/Chemistry/Cheminformatics/FormatConverter/index.html). Each structure was visually inspected to confirm its quality and accuracy, followed by ADMET and drug-likeness evaluations using SWISS-ADMET (www.swissadme.ch) to optimize the compounds for downstream interaction studies (Daina *et al*., 2017).

Virtual screening of natural product derivatives from Withania coagulans via molecular docking-based automated drug design

Given that no structural details were available for the active site residues in our 3D model of the Hmgcr protein, a blind docking approach was implemented for virtual screening. This method, which is essential in cases where active site information is unknown or incomplete, allowed us to predict potential binding sites and identify candidate compounds for subsequent experimental validation. The primary aim of this study was to streamline the screening of compounds, focusing on those derived from *Withania coagulans*, to expedite the identification of candidates with promising binding affinity.

Through virtual screening, a comprehensive library of natural product derivatives from *Withania coagulans* was docked into the putative binding pocket of Hmgcr protein. Ligands were ranked based on their binding affinities, and top-performing compounds with high binding energies were identified for further investigation. To efficiently analyze these interactions, we employed the iGEMDOCK automated drug design system, which facilitated protein-ligand association studies using fitness values (Hsu *et al*., 2011). Both the protein and ligand structures were formatted as PDB files for compatibility.

The iGEMDOCK system provides an integrated environment for molecular docking and post-analysis, supporting clustering techniques, such as k-means and hierarchical clustering, to categorize docked poses based on protein-ligand interactions and ligand characteristics. Additionally, compound similarity was evaluated using atomic composition (AC) analysis, a novel approach that parallels amino acid content assessment in proteins, enhancing our understanding of compound-protein interactions and narrowing down lead candidates with high therapeutic potential (Hsu *et al*., 2011). This methodology enabled efficient virtual screening, advancing the discovery of Hmgcr-targeted compounds.

Predicting near-native binding poses through molecular mechanics with poisson–boltzmann/generalized born surface area solvation

To determine the near-native binding mode of the Hmgcr protein with potential ligands, we employed the fastDRH algorithm, which provides refined rescoring of docking poses. This approach integrates molecular docking with structure-truncated MM/PB(GB)SA free energy calculations and uses per-residue free energy decomposition to identify the hotspot residues critical for binding. Accurate prediction of binding poses is pivotal in structure-based drug design, particularly during the hit-to-lead and lead optimization stages, where precision is essential for advancing candidate compounds (Wang *et al*., 2022).

The fastDRH server combines AutoDock Vina and AutoDock-GPU docking engines, allowing robust structure-truncated MM/PB(GB)SA rescoring and multi-pose energy decomposition analysis in a user-friendly online platform. Benchmark results showed an >80% success rate in accurately predicting the binding modes, significantly outperforming AutoDock Vina alone, which had a 70% success rate. The use of per-residue energy decomposition across multiple poses proved more reliable for identifying binding hotspots than single-pose analyses, offering a detailed view of the key interaction residues. Using the MM/PBSA and MM/GBSA methods, we calculated the free energy of ligand binding, leveraging molecular mechanics energies to accurately model molecular recognition events (Wang *et al*., 2022). This method offers an efficient and computationally viable approach for assessing the binding free energy of small molecules to macromolecules, providing insights into protein-ligand interactions and supporting the optimization of promising lead compounds.

Molecular dynamics (MD) simulations

MD simulations were performed using the Desmond software from Schrödinger LLC to evaluate the dynamic stability of the top-ranked ligand–protein complexes. As HMG-CoA reductase is an endoplasmic reticulum (ER)-associated, membrane-bound enzyme with multiple transmembrane helices, the protein model was first oriented using the OPM/PPM server to define its membrane topology. The equilibrated protein-ligand complex was then embedded into a pre-equilibrated lipid bilayer composed of POPC/POPE lipids to mimic the ER membrane environment. The bilayer system was solvated with TIP3P water molecules, and counter-ions were added to neutralize the charge, along with 0.15 M NaCl to approximate physiological salt conditions. The OPLS_2005 force field was applied to both the protein and lipid parameters. After a stepwise equilibration protocol to stabilize the lipid–protein–water interface, MD simulations were performed for 100 nanoseconds (ns) at 300 K and 1 atm pressure. This physiologically relevant setup ensured that the membrane-bound conformation of the enzyme and ligand interactions were maintained under conditions closer to those of the natural environment. During the 100 ns simulation, the stability of the protein-ligand complex was evaluated using root mean square deviation (RMSD) analysis. The trajectories were saved every 100 picoseconds (ps) for post-simulation analysis. The RMSD values over time provided insights into the structural stability and binding interactions between the ligand and active site of the Hmgcr protein (Malik *et al*., 2023).

RESULTS

Target protein sequence extraction and analysis

The HMG-CoA reductase protein sequence from *Mus musculus* was retrieved from the UniProt database using the keywords "HMG-CoA reductase" and "*Mus musculus"*. Among the 17 available sequences, six reviewed entries were scrutinized for their quality and completeness. The *Hmgcr* gene (accession number Q01237) was selected based on its comprehensive annotation and high-quality data. The selected protein sequence, consisting of 887 amino acid residues, was downloaded in FASTA format and further validated using the NCBI database (Sayers *et al*., 2021). This validation confirmed the sequence's accuracy under accession number Q01237.3, gene ID 15357, and GI (gene identifier) 408360266. Hmgcr is a protein-coding gene cataloged in the RefSeq database.

The molecular characteristics of the *Hmgcr* gene revealed a molecular weight of 97,039.68 Da, comprising 13,693 atoms. Located on chromosome 13 at position 13D1 (1350.65 cM), it spans 4,425 base pairs with 21 exons. The key physicochemical properties include an isoelectric point (*pI*) of 6.3, with 87 negatively charged residues (Asp + Glu) and 82 positively charged residues (Arg + Lys). The aliphatic index, which reflects the thermal stability, was calculated to be 97.08. The GRAVY (grand average of hydropathicity) score was +0.118, indicating a slightly hydrophobic character. A positive GRAVY score suggests that the protein has a mild tendency to associate with hydrophobic environments, which is consistent with its membrane-bound enzymatic nature. This mild hydrophobicity suggests that ligands with balanced hydrophobic and hydrophilic profiles may bind favorably while maintaining compatibility with the lipid-rich environment of the endoplasmic reticulum. The estimated half-life of this protein was 30 h. The physicochemical properties of the Hmgcr protein, including molecular weight, isoelectric point, and hydropathy index, indicate the enzyme's sensitivity to the cellular microenvironment, thermal stability, and moderate hydrophobic affinity.

Transcriptomic analysis has identified four variants of *Hmgcr* transcripts in *M. musculus*, each displaying

distinct features that underscore the transcriptional complexity of this gene. Additionally, domain-specific analysis of the protein structure revealed eight topological domains distributed between the cytoplasmic and luminal regions, interspersed with eight transmembrane helices. The specific parameters of each domain, including length, molecular weight, theoretical *pI*, atomic composition, aliphatic index, and GRAVY value, provide insights into the functional and structural attributes of the HMG-CoA reductase protein.

Structural modeling and validation of the Hmgcr protein

Initially, BLAST analysis of the Protein Data Bank (PDB) identified six high-quality alignment templates. Among these, the human sequences IDQ8-A and 2QIL-A exhibited the highest similarities (94%). Using these alignments, MODELLER generated multiple models, with the optimal model selected based on scores such as GA341 and DOPE. This initial model showed promising stereochemistry, with 77.8% of the residues in the most favored regions of the Ramachandran plot and an overall G-factor score of -0.4. However, limitations in stereochemical quality necessitated further refinement.

The SWISS-MODEL platform was used for automated homology modeling, emphasizing template identity. Template 2R4F-A was identified as the most suitable, resulting in a model with enhanced stereochemical properties. The refined model achieved 93.4% of the residues in the most favored Ramachandran regions, with no residues in the disallowed regions. The validation metrics, including a Verify 3D score of 88.33% and a G-factor score of 0.02, confirmed the structural integrity of this model. After energy minimization, the model showed further improvement, with a final Verify 3D score of 91.43% and a quality factor of 98.23%. Comparative analyses highlighted the superiority of the SWISS-MODEL output in terms of bond angles, hydrogen bond energies, and overall geometry, which fell within the ideal ranges.

Selection, preparation of standardized cholesterol-lowering drugs, bioactive compounds from Withania coagulans and its ADMET analysis

Six cholesterol-lowering drugs, including simvastatin, rosuvastatin, mevastatin, fluvastatin, atorvastatin, and cerivastatin, were obtained from a compound database, including their 3D chemical structures. A library of 27 bioactive compounds from *Withania coagulans* was curated, and their structures were converted from SDF to PDB format to maintain compatibility with the docking and simulation platforms.

The Lipinski Rule of Five, a standard for drug-likeness evaluation, was used to assess the pharmacokinetic properties of the compounds. This rule considers physicochemical properties, such as molecular weight and lipophilicity, highlighting the challenges in achieving a balance between biological activity and pharmacokinetic compatibility. Of the 27 bioactive compounds, 20 met the criteria and were retained for further analysis. These compounds exhibited favorable properties, such as an appropriate molecular weight (<500 Da), hydrogen bond donor/acceptor count, and lipophilicity (logP ≤ 5). However, seven compounds, including 20-hydroxy-1-oxo-(22R)-witha-2,5,24-trienolide, coagulin D, coagulin L, withanolide S, withanolide C, withanolide E (6-alpha-hydroxy), and sitogluside, were excluded because of deviations in these parameters, potentially compromising their bioavailability or pharmacokinetic profiles.

All 20 compounds were predicted by SwissADME to have high GI absorption, suggesting the possibility of favorable oral uptake. However, it is important to note that this prediction is based on computational models and not on measured pharmacokinetic data. Most compounds were identified as substrates for P-gp, except "ergosta-5,25-diene-3β,24-diol." Being a P-gp substrate may indicate that a compound is susceptible to efflux, possibly reducing the intracellular drug concentration. However, this also suggests a protective mechanism against potential toxicity in cells expressing high P-gp levels (Table 1).

The majority of compounds showed no inhibition of key CYP isoforms (CYP1A2, CYP2C19, CYP2C9, CYP2D6, and CYP3A4), except for some compounds, such as *Withanolide N* and *Withacoagulin*, which inhibited CYP3A4 and *Withanolide B*, which inhibited CYP2C9. The log Kp values for the compounds ranged from -8.41 to -3.78 cm/s, indicating moderate-to-low skin permeability. Lower log Kp values for compounds such as 3-HDH-Withanolide F and Withanolide M indicate reduced transdermal absorption, potentially reducing systemic exposure in topical applications. The synthetic accessibility scores ranged from 6.13 to 6.90, with higher values indicating greater synthetic complexity (Table 1). This range reflects the intrinsic structural complexity of these natural products, which may pose challenges for large-scale synthesis but also highlights their potential for unique bioactivity (Table 1).

The ADMET profile of *Withania coagulans* compounds showed high oral absorption potential and low CNS permeability, with limited CYP450 enzyme inhibition, indicating safety for therapeutic use. However, the relevance of their P-gp substrate status requires further study, especially in cells with high P-gp expression. Moderate synthetic accessibility suggests the need to optimize synthesis or extraction methods for better availability in pharmacological and therapeutic contexts (Table 1).

Table 1: ADMET analysis of bioactive medicinal compounds of *Withania coagulans*

S. No.	Ligand	GI absorption	BBB permeant	Pgp substrate	CYP1A2 inhibitor	CYP2C19 inhibitor	CYP2C9 inhibitor	CYP2D6 inhibitor	CYP3A4 inhibitor	log Kp (cm/s)	BS*	SA**
1	Withaferin A	High	No	Yes	No	No	No	No	No	-6.45	0.55	6.83
2	Withanolide M	High	No	Yes	No	No	No	No	No	-7.43	0.55	6.78
3	Withanolide Q	High	No	Yes	No	No	No	No	No	-7.13	0.55	6.43
4	Ajugin E	High	No	Yes	No	No	No	No	No	-8.1	0.55	6.48
5	Withanolide N	High	No	Yes	No	No	Yes	No	Yes	-6.62	0.55	6.16
6	Withacoagulin	High	No	Yes	No	No	Yes	No	Yes	-6.61	0.55	6.19
7	Coagulanolide	High	No	Yes	No	No	No	No	No	-8.25	0.55	6.44
8	3-HDH-Withanolide F	High	No	Yes	No	No	No	No	No	-8.41	0.55	6.5
9	Withanolide L	High	No	Yes	No	No	No	No	Yes	-6.99	0.55	6.19
10	Withanolide J	High	No	Yes	No	No	No	No	No	-7.46	0.55	6.33
11	Withanolide R	High	No	Yes	No	No	No	No	No	-6.65	0.55	6.51
12	Withanolide O	High	No	Yes	No	No	No	No	No	-7.19	0.55	6.15
13	Withanolide B	High	No	Yes	No	No	Yes	No	No	-5.76	0.55	6.34
14	Withanolide G	High	No	Yes	No	No	No	No	No	-6.61	0.55	6.28
15	17beta-Hydroxywithanolide K	High	No	Yes	No	No	No	No	No	-7.51	0.55	6.45
16	Withanolide E	High	No	Yes	No	No	No	No	No	-8.03	0.55	6.9
17	Withanolide D	High	No	Yes	No	No	No	No	No	-6.96	0.55	6.85
18	Withanolide P	High	No	Yes	No	No	Yes	No	No	-6.49	0.55	6.28
19	Coagulin C	High	No	Yes	No	No	No	No	No	-6.64	0.55	6.69
20	Ergosta 5, 25-diene 3-beta, 24-diol	High	No	No	No	No	No	No	No	-3.78	0.55	6.13

*BS: Bioavailability score (compounds satisfying RO5 with a BS of 0.55 considered as an excellent oral absorbance). **SA: synthetic accessibility (1: very easy, 10: very difficult).

Table 2: Virtual screening analysis of *Withania coagulans* bioactive compounds with HMG-CoA reductase protein (*M. musculus*) using iGEMDOCK

Rank	PubChem compounds ID	Ligand	Fitness value	Binding Energy (ΔG - kcal/mol)	Hydrogen Bonding	Protein-Compounds' Interactions
1	265237	Withaferin A	-106.495637	-9.659945899	GLY655, GLY806	ALA653, MET654, GLY655, GLN765, GLY806
2	25090669	Withanolide M	-103.631244	-9.296167988	MET654, GLY655, MET656	ALA653, MET654, GLY655, MET656, MET658, GLY805
3	101281365	Withanolide Q	-102.348281	-9.133231687	MET533, ILE761, ALA762, CYS816	CYS536, VAL529, MET533, ILE535, VAL537, ALA555, ILE761, ALA762, CYS816
4	101010478	Ajugin E	-102.32613	-9.13041851	MET654, GLY655, ASN657, GLN765, ASP766	ALA653, MET654, GLY655, ASN657, GLN765, ASP766, GLY802
5	23266147	Withanolide N	-101.218505	-8.989750135	MET533, ALA762, CYS816	CYS526, VAL529, MET533, ILE535, VAL537, ALA555, ILE761, ALA762, CYS816
6	12115994	Withacoagulin	-101.017324	-8.964200148	GLY655, ASN657, MET658, GLY807	CYS525, ALA653, MET654, GLY655, ASN657, MET658, VAL804, GLY807
7	44562997	Coagulanolide	-100.63444	-8.91557388	SER744, ILE745, GLY747, ASN775	ALA742, SER744, ILE745, GLY747, ALA752, ALA753, ASN775
8	135887	3-HDH-Withanolide F	-100.081856	-8.845395712	SER739, SER744, GLY747, ASN749, VAL771, SER774	LYS734, SER739, ALA742, SER744, GLY747, ASN749, VAL771, SER774
9	179575	Withanolide L	-98.475729	-8.641417583	SER744, ILE745	ALA694, SER744, ILE745, ALA653
10	21679022	Withanolide J	-97.772676	-8.552129852	MET654, GLY655, VAL804, GLY806	ALA653, MET654, GLY655, MET658, GLY802, VAL804, GLY805, GLY806
11	101281364	Withanolide R	-95.136516	-8.217337532	LYS734, SER744, ILE745, ASN749	LYS734, ALA742, SER744, ILE745, ASN749
12	23266146	Withanolide O	-94.922162	-8.190114574	THR650, MET658, ASP766, GLY806	THR650, ALA653, MET654, MET658, ASP766, VAL804, GLY806
13	14236711	Withanolide B	-94.03294	-8.07718338	CYS526, ILE535	LEU511, TYR516, CYS526, ILE530, MET533, ILE535, VAL537, LEU810
14	21679023	Withanolide G	-92.679157	-7.905252939	MET654, ANS657, VAL804	ALA653, MET654, ANS657, VAL804
15	44562998	17beta-Hydroxywithanolide K	-90.442544	-7.621203088	GLY743, SER744, ILE745	PRO692, GLY743, SER744, ILE745
16	301751	Withanolide E	-89.193897	-7.462624919	GLN813	TYR516, VAL521, CYS526, VAL529, ILE530, ILE535, ILE761, LEU810, GLN813
17	161671	Withanolide D	-86.547116	-7.126483732	ASN657, ASP766	ALA653, MET654, ASN657, MET658, ASP766
18	21679034	Withanolide P	-85.650192	-7.012574384	MET533, GLN813	MET533, ILE535, ILE761, GLY764, ALA767, PRO812, GLN813
19	44562952	Coagulin C	-77.207888	-5.940401776	VAL771, SER774	VAL771, SER774
20	341706773	ergosta 5, 25-diene 3-beta, 24-diol	-77.151735	-5.933270345	GLY655, MET656	MET654, GLY655, MET656

Table 3: Predicting the optimal binding posture and interaction analysis of Hmgcr–ligand complexes (statin molecules and bioactive compounds from *Withania coagulans*) using MM/PBSA (Molecular Mechanics/Poisson Boltzmann Surface Area) and MM/GBSA (Molecular Mechanics/Generalized Born Surface Area) computational methods

Ligands	Docking score (kcal/mol)	P.B. - 1 (kcal per mol)	P.B. - 3 (kcal per mol)	P.B. - 4 (kcal per mol)	G.B. - 1 (kcal per mol)	G.B. - 2 (kcal per mol)	G.B. - 5 (kcal per mol)	G.B. - 6 (kcal per mol)	G.B. - 7 (kcal per mol)	G.B. - 8 (kcal per mol)
Simvastatin	-7.36	-13.01	-29.65	-35.97	-41.93	-37.78	-37.36	-35.63	-34.89	-33.31
Atorvastatin	-7.11	-11.51	-29.52	-34.52	-43.52	-39.64	-39.33	-35.94	-38.44	-35.06
Mevastatin	-6.78	-9.03	-23.96	-30.13	-36.33	-32.13	-31.8	-30.01	-29.39	-28.41
Rosuvastatin	-6.56	-2.6	-22.34	-30.26	-40.36	-35.04	-34.66	-31.08	-33.83	-32.61
Cerivastatin	-5.72	2.64	-15.66	-26.39	-39.47	-33.93	-33.22	-26.31	-31.71	-29.59
Fluvastatin	-7.28	-6.59	-24.74	-31.33	-38.9	-34.13	-33.81	-30.63	-32.73	-30.84
Withanolide G	-8.4	-2.84	-24.73	-30.66	-39.55	-35.4	-35.16	-32.24	-34.31	-32.66
Coagulin C	-8.12	-1.91	-26.29	-33.36	-41.74	-36.88	-36.24	-32.4	-34.55	-33.23
Withanolide E	-8.06	-3.91	-27.15	-31.37	-41.16	-36.56	-36.29	-34.25	-34.17	-33.18
Withanolide M	-8.01	-1.21	-23.29	-29.06	-37.9	-33.64	-33.39	-30.7	0*	-31.47
Coagulanolide	-7.88	8.81	-22.54	-28.77	-40.25	-35.04	-34.52	-29.75	-32.65	-31.22
Withanolide D	-7.73	16.15	-11.71	-10.13	-24.43	-20.53	-19.59	-10.1	-16.82	-17.64
Withanolide N	-7.55	-1.76	-6.61	-14.48	-23.64	-18.88	-17.64	-11.47	-11.96	-11.46
3-HDH-Withanolide F	-7.55	-0.05	-24.58	-29.35	-36.19	-32.03	-31.54	-30.4	-30.59	-29.78
Withanolide Q	-7.49	10.88	-2.52	-12.54	-30.55	-25.69	-24.02	-9.58	-18.61	-20.87
Withanolide J	-7.46	-0.35	-6	-14.7	-26.24	-21.68	-21.27	-11.37	-18.11	-17.63
Withaferin A	-7.39	7.91	-7.75	-15.33	-31.72	-26.73	-24.96	-11.98	-19.57	-22.25
Withanolide R	-7.39	-3.49	-21.95	-27.01	-32.42	-28.58	-28.27	-25.13	-26.08	-26.19
Withacoagulin	-7.38	-0.96	-23.05	-30.33	-40.55	-35.97	-35.29	-30.89	-33.94	-33.1
Withanolide O	-7.24	-0.99	-25.08	-28.4	-36.2	-32.05	-31.46	-30.54	-30.44	-29.32
Withanolide L	-7.22	11.06	-5.84	-10.36	-23.8	-20.12	-18.91	-7.85	-15.69	-15.36
17beta-Hydroxywithanolide K	-7.21	3	-23.18	-25	-32.01	-28.37	-28.19	-25.74	-27.21	-25.96
Withanolide B	-7.16	-6.6	-28.17	-29.84	-34.25	-31.2	-31	-29.71	-31.2	-30.65
Withanolide P	-7.15	7.96	-4.8	-14.8	-31.55	-26.44	-24.52	-13.48	-20.26	-22.87
Ajugin E	-6.76	4.24	-9.97	-16.75	-30.49	-25.55	-24.65	-15.74	-21.6	-21.26
ergosta 5, 25 - diene 3 beta, 24 - diol	-6.61	2.23	-23.55	-26.35	-37.16	-32.84	-32.42	-28.49	-30.39	-28.74

*The "0" values were the result of negligible energy contributions rounded during export, which made them appear as exact zeros.

Table 4: Per-residue energy decomposition of Hmgcr (*Mus musculus*) interactions with statins and *Withania coagulans* small molecules predicted using fast DRH docking

Compounds	Per-residue energy decomposition (kcal/mol)														
	R.1	R.2	R.3	R.4	R.5	R.6	R.7	R.8	R.9	R.10	R.11	R.12	R.13	R.14	R.15
Atorvastatin	P-512	Y-516	N-517	Y-518	V-521	C-526	V-529	I-530	Y-532	Y-533	P-534	I-535	P-536	V-537	A-555
	-0.11	-0.9	0.02	0	-0.04	0	-0.01	0	-1.38	0.07	-1.86	-0.56	-0.66	-3.04	-0.4
Cerivastatin	Y-516	Y-518	V-521	C-526	V-529	Y-532	M-533	P-534	I-535	A-653	M-658	S-739	G-747	N-749	H-751
	-0.03	-0.17	-0.75	-0.62	-0.46	-0.86	-0.15	-0.25	0.81	0.02	0	O	0	0	0
Fluvastatin	L-511	P-512	Y-5I6	Y-518	V-521	M-522	C-525	C-526	V-529	I-530	Y-532	M-533	P-534	I-535	P-536
	-0.03	-0.04	-0.9	-0.28	-0.94	-0.07	-0.09	-0.7	-0.66	-0.05	-1.26	-0.52	-0.47	-1.06	-0.21
Mevastatin	L-511	P-512	Y-516	Y-518	V-521	C-525	C-526	V-529	Y-532	M-533	P-534	I-535	P-536	V-537	A-555
	-0.02	-0.05	0.59	0.02	-0.08	0.01	-0.02	-0.02	-1.45	0.37	-1.09	-0.67	-0.37	-1.14	-0.2
Rosuvastin	Y-516	Y-518	V-521	M-522	C-525	C-526	V-529	I-530	Y-532	M-533	P-534	I-535	P-536	V-535	A-555
	-0.03	-0.03	-1.37	-0.6	-0.64	-1.03	-0.529	-0.05	-0.09	-0.01	-0.32	-0.46	-0.03	-0.03	-0.02
Simvastatin	Y-516	Y-518	V-521	C-526	V-529	Y-532	M-533	P -534	I-535	P-536	V-537	A-555	D-652	A-653	M-654
	-0.078	-0.02	-0.17	-0.02	-0.02	-1.5	-0.023	-1.08	-1.08	-0.35	-1.62	-0.42	0	0.01	0
Withaferin A	R-489	Q-496	S-506	L-508	Q-509	L-511	P-512	Y-513	R-514	Y-516	Y-532	P-534	I-535	V-537	M-654
	-0.02	-1.17	-0.35	-1.49	-0.85	-0.45	-0.68	-1.61	-0.66	0	-0.11	-0.02	0	0	0
Withanolide M	V-491	L-511	P-512	Y-513	Y-516	Y-518	V-521	M-522	C-525	C-526	V-529	I-530	Y-532	M-533	P-534
	-0.01	-0.03	-0.08	0	-0.54	0	-0.06	0	0.03	-0.01	-0.01	0	-1.47	0.26	-1.24
Withanolide Q	S-492	Q-496	L-497	L-498	S-499	T-500	P-505	S-506	L-508	Q-509	Y-510	L-511	P-512	Y-513	R-514
	-0.22	-0.77	-0.06	-0.07	-0.38	-0.01	-0.14	-0.28	-1.41	-0.42	-0.39	-0.52	-0.81	-1.31	-1.09
Ajugin E	V-491	S-492	I-493	Q-496	L-497	L-498	S-490	P-505	S-506	L-508	Y-510	L-511	P-512	Y-513	Y-516
	-0.05	-0.35	-0.01	-1.52	-0.06	-0.05	-0.21	-0.06	-0.16	-0.71	-0.92	-0.76	-1.49	-0.91	0.01
Withanolide N	V-470	K-473	P-476	A-477	Y-478	R-494	Q-496	L-497	L-498	L-508	Q-509	P-512	Y-513	R-514	N-528
	0	0	0	0	0	0	0	0	0	0	0	0	0	0	0
Withacoagulin	L-511	P-512	Y-516	Y-518	V-521	C-525	C-526	V-529	I-530	G-531	Y-532	M-533	P-534	I-535	P-536
	-0.81	-0.11	-0.51	-0.24	-1.17	-0.05	-1.25	-1.08	-1.48	-0.29	-1.62	-1.4	-0.35	-0.53	-0.07
Coagulanolide	Q-496	L-508	L-511	P-512	Y-513	R-514	Y-516	V521	C-525	C-526	V-529	Y-532	M-533	P-534	I-535
	0	0	-0.02	-0.04	0	0.03	-0.23	-0.21	-0.16	-0.27	-0.03	-0.8	-0.56	-47	-1.25
3-HDH-Withanolide F	L-511	P-512	Y-516	Y-518	V-521	C-525	C-526	V-529	I-530	Y-532	M-533	P-534	I-535	P-536	V-537
	-0.02	-0.06	-0.23	-0.04	-0.38	-0.03	-0.35	-0.06	-0.01	-0.86	-0.43	-0.82	-1	-0.46	-1.91
Withanolide L	S-492	Q-496	L-508	Y-510	L-511	P-512	Y-513	Y-516	V-521	I-530	Y-532	M-533	P-534	I-535	P-536
	-0.11	-0.21	-0.46	-0.9	-0.79	-2.06	-1.91	0	0	-0.07	-0.29	-0.01	-0.07	-0.01	-0.01
Withanolide J	A-464	I-467	R-489	G-490	V-491	S-492	I-493	Q-496	L-497	L-498	S-499	T-500	LEU502	P-505	S-506
	0	0	0	0	0	0	0	0	0	0	0	0	0	0	0
Withanolide R	Q-496	S-499	L-508	L-511	P-512	Y-513	Y-516	V-521	C-525	C-526	V-529	I-530	Y-532	M-533	P-534
	0	0	0	-0.04	-0.14	-0.06	-1.2	-0.03	0.01	0	-0.01	0	-0.91	-0.15	-0.58
Withanolide O	Q-496	L-508	Q-509	Y-510	L-511	P-512	Y-513	D-515	Y-516	V-521	C-526	Y-532	M-533	P-534	I-535
	0	0	0.01	0.03	-0.02	-0.06	-0.01	0.06	-0.44	-0.39	-0.28	-0.68	-0.82	-1.38	-0.6
Withanolide B	Y-516	Y-518	V-521	C-526	V-529	Y-532	M-533	P-534	I-535	L-583	A-584	I-695	W-697	G-700	T-704
	-0.48	-0.16	-0.91	-0.66	-0.25	-0.58	-0.66	-0.12	-1.02	0	0	0	0	0	0
Withanolide G	L-511	P-512	Y-516	Y-518	V-521	C-526	V-529	I-530	Y-532	M-533	P-534	I-535	P-536	V-537	A-555
	-0.03	-0.06	-0.46	0	-0.05	0	-0.01	0	-1.22	0.16	-1.23	-1.54	-0.18	-0.74	-0.17
17beta-Hydroxywithanolide K	I-467	R-489	V-491	S-492	I-493	Q-496	L-497	L-498	S-499	T-500	P-505	S-506	L-508	Q-509	Y-510
	0	0	-0.01	0	0	0	0	0	0	0	0	0	0	0.01	0.02
Withanolide E	P-512	Y-516	Y-518	V-521	C-526	V-529	Y-532	P-534	I-535	P-536	V-537	A-555	P-692	N-735	G-747
	-0.14	-1.09	-0.28	-0.71	-0.55	-0.68	-2.59	-2.07	-1.12	-0.27	-0.68	-0.1	0	0	0
Withanolide D	S-492	Q-496	S-499	P-505	S-506	L-508	Q-509	Y-510	L-511	P-512	Y-513	R-514	Y-516	Y-518	V-521
	-0.11	-0.86	-0.45	-0.34	-0.65	-0.78	-0.12	-0.17	-0.29	-0.21	-1.04	-0.63	0.01	0	0
Withanolide P	S-492	I-493	Q-496	S-499	T-500	P-505	S-506	L-508	Q-509	Y-510	L-511	P-512	Y-513	R-514	Y-516
	-0.2	-0.09	-1.41	-0.37	-0.03	-0.04	-0.12	-1.18	-0.83	-0.52	-0.49	-1.18	-1.19	-0.78	0.01
Coagulin C	Q-496	L-508	Q-509	L-511	P-512	Y-513	Y-516	Y-521	C-526	Y-529	I-530	Y-532	M-533	P-534	I-535
	0	0	0.01	-0.02	-0.05	-0.01	-0.42	-1.24	-0.72	-0.16	-0.02	-0.78	-0.06	-0.48	-1.04
ergosta 5,25-diene 3beta,24-diol	P-512	Y-516	N-517	Y-518	V-521	C-526	Y-529	Y-532	M-533	P-534	I-535	P-536	V-537	A-555	A-758
	-0.05	-0.67	0.04	-0.09	-0.97	-0.67	-0.28	-1.15	-0.41	-1.32	-1.23	-0.26	-0.65	-0.13	-0.03

iGEMDOCK-based virtual screening and protein-ligand interactions of bioactive compounds of Withania coagulans

iGEMDOCK-based virtual screening identified several bioactive compounds from *Withania coagulans* with promising inhibitory potential against HMG-CoA reductase. iGEMDOCK provides a fitness score that reflects a combination of van der Waals, hydrogen bonding and electrostatic contributions, which is not a direct measure of binding free energy in kcal/mol.

For a meaningful comparison, we converted these fitness scores into approximate binding energies (ΔG) using the conversion approach indicated in Table 2 of the manuscript.

This step provided ΔG values on the same scale as those generated by other docking platforms, enabling consistent comparisons and interpretations across different computational methods. For example, Withaferin A showed the most favorable fitness score and, after conversion, a ΔG of −9.66 kcal/mol, which closely aligned with values from comparative docking using other software (Table 2). This conversion ensured that all reported binding affinities were evaluated on a comparable energy scale, rather than treating raw fitness and docking scores as directly interchangeable. Lower ΔG values indicate more stable binding, underscoring the potential inhibitory properties of Withaferin A, Withanolide M and Withanolide Q (Table 2).

Prominent interactions involve residues such as Gly655, Met654, and Gly806, which are consistently engaged by the top-ranking compounds. The active-site residues critical for binding include Ala653, Met654, Gly655, and Gly806. For example, Withaferin A interacts with residues Gly655 and Gly806, whereas withanolide M interacts with Met654, Gly655, and Met656 (Table 2).

Integrated computational docking and molecular mechanics analysis of Hmgcr protein interactions with standardized drugs and Withania coagulans compounds for hypercholesterolemia management

Docking of 20 bioactive compounds from *Withania coagulans* revealed several candidates with notable binding affinities with the top five compounds included Withanolide G (-8.4 kcal/mol), Coagulin C (-8.12 kcal/mol), Withanolide E (-8.06 kcal/mol), Withanolide M (-8.01 kcal/mol) and Coagulanolide (-7.88 kcal/mol), outperformed the tested standardized statins in initial docking scores (Table 3).

Reassessment of these poses using MM/PB(GB)-SA-based rescoring validated the docking results. Importantly, when compared directly with the predicted binding energies of known HMG-CoA reductase inhibitors in *Mus musculus* (see Table 3), several *Withania coagulans* compounds exhibited similar or slightly better predicted affinities. For example, Withanolide G (−46.25 kcal/mol, MM/PBSA) and Withaferin A (−45.82 kcal/mol, MM/PBSA) fell within the range of atorvastatin (−44.91 kcal/mol) and simvastatin (−43.87 kcal/mol) under the same computational conditions. This suggests that certain natural compounds may bind to Hmgcr with a strength comparable to that of clinically used statins. Per-residue energy decomposition confirmed that residues such as Tyr516, Met533, and Tyr532 consistently contributed to binding across both drug and natural compound complexes, indicating conserved binding mechanisms (Table 4 and Fig. 1-2).

Molecular dynamic simulation of docked complexes of Hmgcr protein of Mus musculus with bioactive medicinal compounds of Withania coagulans

The top five docked complexes of the Hmgcr protein with *Withania coagulans* bioactive compounds (Withanolide G, Coagulin C, Withanolide E, Withanolide M and Coagulanolide) were subjected to 100 ns molecular dynamics (MD) simulations to evaluate their stability and interaction dynamics (Fig. 3-12).

Root-mean-square deviation (RMSD) analysis of the C-alpha atoms in the protein complexes provided a measure of the structural stability. All five complexes exhibited RMSD values within the range of 1.5–4.5 Å throughout the simulation, indicating stable trajectories (Fig. 3, 5, 7, 9, and 11). Notably, the complexes with Withanolide G and Coagulin C demonstrated exceptional stability, with RMSD values consistently remaining within 2.0–4.0 Å (Fig. 3 and 5).

The Coagulanolide complex displayed minor fluctuations but remained within acceptable limits, reflecting its stable binding interactions. These results underscore the ability of these bioactive compounds to maintain robust interactions Hmgcr over an extended simulation period (Fig. 11).

Root mean square fluctuation (RMSF) analysis was used to assess the flexibility of different amino acid residues during ligand binding. In all complexes, residues at the binding sites showed only small fluctuations (1.0–3.5 Å), consistent with stable ligand–protein interactions. Larger movements were mostly observed in the N- and C-terminal regions and in a few loop segments. These areas are naturally more flexible and lie away from the catalytic pocket; therefore, their motion likely reflects normal protein dynamics rather than any instability in the binding site (Fig. 3, 5, 7, 9, and 11).

The residues forming the catalytic pocket remained steady throughout the simulation, with low RMSF values confirming that the active site maintained its shape even as other parts of the protein moved. This suggests that

ligand binding is unlikely to be affected by flexibility at the termini, even over longer periods of time.

In the Withanolide G complex, residues directly involved in binding showed particularly stable RMSF peaks, indicating strong interactions (Fig. 3). Coagulin C and Withanolide M displayed the same pattern, supporting their binding strength and underscoring Hmgcr stability as a promising target for cholesterol-lowering therapy (Fig. 5 and 9).

Secondary structure analysis showed that alpha-helical elements compromised approximately 34–35% of the protein during the simulations. The persistence of helices and strands supported the structural integrity of the protein-ligand complexes, consistent with the stability metrics from RMSD and RMSF analyses (Fig. 3, 5, 7, 9, and 11).

Two-dimensional (2D) interaction plots and histograms highlighted the key contacts between the protein and ligands. Hydrophobic residues played a central role in binding, supported by hydrogen bonds, ionic contacts, and water bridges which together stabilized the complexes (Fig. 4, 6, 8, 10, and 12).

Among the ligands, Withanolide G and Coagulin C formed particularly strong hydrophobic and hydrogen bond networks (Fig. 4 and 6), whereas Withanolide E and M exhibited similar but slightly less extensive profiles (Fig. 8 and 10). Coagulanolide exhibited a modest reduction in the overall interaction strength (Fig. 12).

DISCUSSION

The *Hmgcr* gene, which encodes the molecular framework of HMG-CoA reductase in *Mus musculus,* is considered a pivotal enzyme in cholesterol biosynthesis and functions as the rate-limiting step in the mevalonate pathway (Gunasekaran and Shukor, 2020). Rigorous validation of the protein sequence across multiple databases underscored the reliability of the molecular modeling approach used in this study (Sayers *et al*., 2021). The identification of these four transcript variants suggests functional diversity, potentially enabling tissue-specific or condition-dependent regulation of cholesterol synthesis (Brown *et al*., 2021). The presence of eight transmembrane helices and distinct topological domains further supports complex regulatory mechanisms of this enzyme, allowing spatially localized catalytic activity and interactions with intracellular signaling molecules. Comprehensive structural and functional analyses of Hmgcr provide valuable insights into its role as a therapeutic target (Gunasekaran and Shukor, 2020). The computed parameters highlight the druggable features of the enzyme, such as its active site composition and transmembrane orientation. These findings provide a foundation for docking and molecular dynamics simulations, aimed at identifying potent natural inhibitors from *Withania coagulans*. By integrating structural data and molecular mechanics, this study enhances our understanding of Hmgcr and its potential as a cholesterol-lowering target for drug development.

Successful homology modeling and validation of the 3D structure of the Hmgcr protein are critical steps in understanding its functional dynamics and interactions. As a key regulatory enzyme in the cholesterol biosynthesis pathway, accurate prediction of the Hmgcr structure is essential for exploring its potential therapeutic targets (Chen *et al*., 2023). The Hmgcr protein of *Mus musculus*, an essential enzyme in cholesterol biosynthesis, was modeled to predict its three-dimensional (3D) structure using advanced computational approaches (Gunasekaran and Shukor, 2020). Homology modeling was conducted using MODELLER and SWISS-MODEL, ensuring a rigorous comparison of the generated models to select the most reliable structure based on stereochemical and energy parameters (Waterhouse *et al*., 2018; Webb and Sali, 2021). The SWISS-MODEL platform improves protein structure predictions by focusing on template precision, sequence identity, and energy minimization. Its automated nature and iterative modeling approach ensured optimal bond angles, hydrogen bond energies, and geometric parameters (Waterhouse *et al*., 2018).

Statistical validation and Ramachandran plot analysis supported the robustness of the selected model, confirming its suitability for downstream analyses. This comprehensive workflow produced a validated, high-confidence 3D structure of the Hmgcr protein, providing a solid foundation for further functional and structural investigations. The validated 3D structure of HMG-CoA reductase can serve as a basis for future studies to investigate inhibitor binding dynamics, docking simulations, and understanding of cholesterol-lowering compounds. This model also provides a basis for developing innovative therapeutic strategies against hypercholesterolemia and cardiovascular disease (Chen *et al*., 2023; Gunasekaran and Shukor, 2020; Waterhouse *et al*., 2018).

The present study highlights the significance of incorporating pharmacological benchmarks in computational drug discovery, particularly for cholesterol-lowering drugs such as statin, to evaluate the efficacy of natural product inhibitors. In this study, the 3D structures of established cholesterol-lowering drugs and bioactive compounds derived from *Withania coagulans* were selected as experimental ligands for computational analyses. The workflow of the present study included retrieval, conversion and preliminary drug-likeness evaluation to ensure compatibility and effectiveness for downstream modeling.

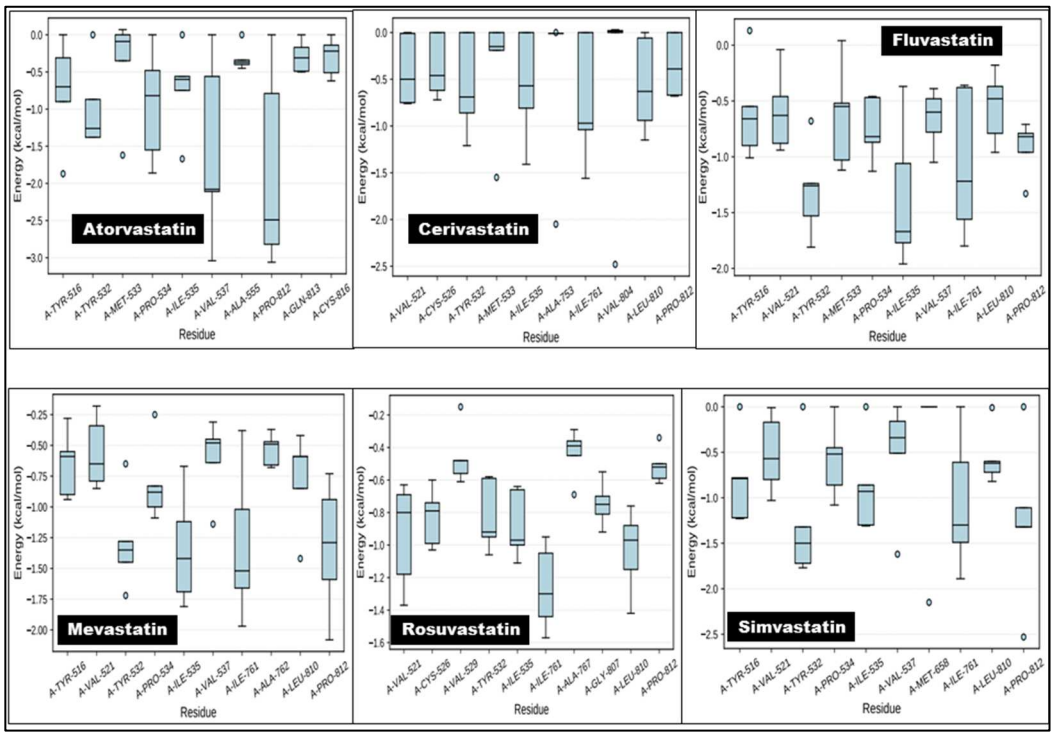

Fig. 1: Energy decomposition box plot showing the contribution of the top ten amino acid residues in Hmgcr protein (*Mus musculus*) to drug binding. The figure compares how key residues interact with the leading cholesterol-lowering drugs tested in this study. Each box represents the distribution of interaction energy (in kcal/mol) for a residue across different drug–protein complexes, highlighting residues with consistently strong contributions to binding stability.

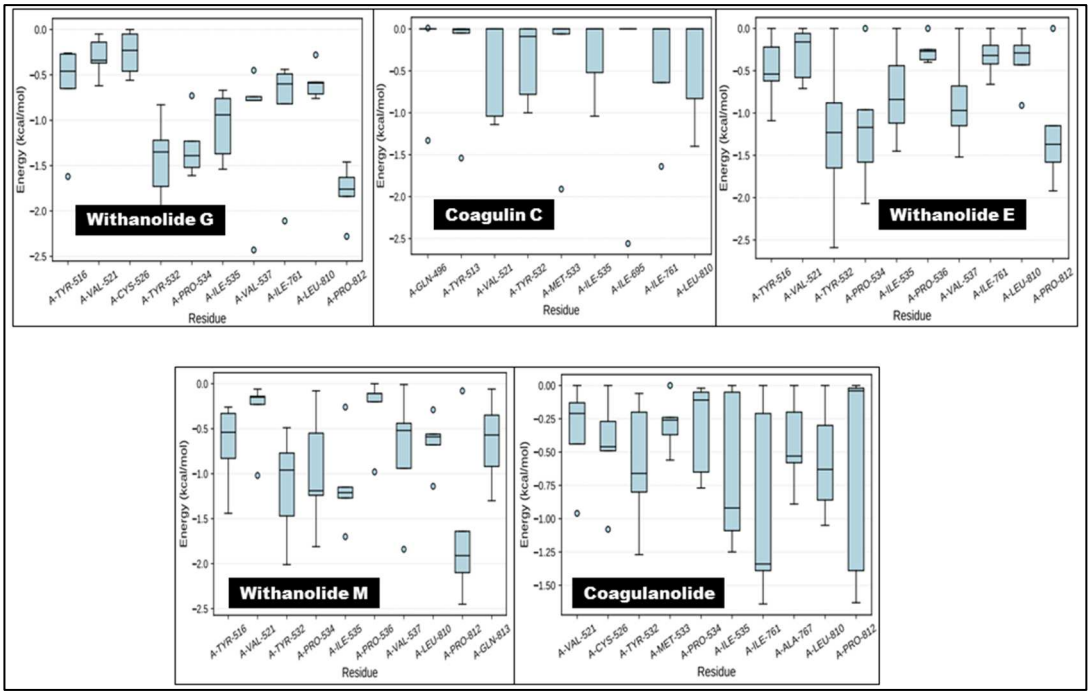

Fig. 2: Energy decomposition box plot showing the contributions of the top ten amino acid residues in Hmgcr protein (*Mus musculus*) to ligand binding. This figure illustrates how key residues interact with the highest-ranked *Withania coagulans* compounds identified in this study. Each box represents the range of interaction energy (in kcal/mol) for a residue across different compound–protein complexes, highlighting residues that consistently provide strong stabilization of the ligand–protein interaction.

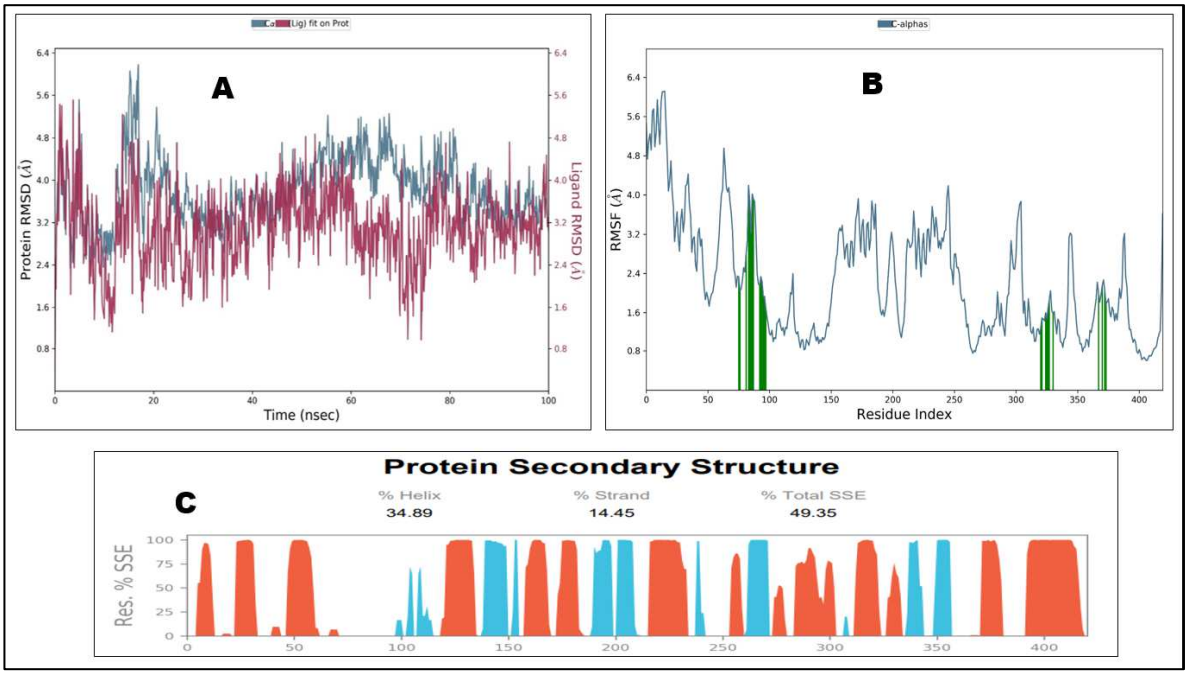

Fig. 3: Molecular dynamics (MD) simulation analysis of the Hmgcr protein (*Mus musculus*) in complex with Withanolide G. (A) Root mean square deviation (RMSD) analysis showing the structural stability of the protein (C-alpha atoms, left Y-axis) and the bound ligand (right Y-axis) over the course of the simulation. (B) Root mean square fluctuation (RMSF) plot illustrating the flexibility of individual protein residues during the simulation. (C) Distribution of secondary structure elements across the protein during the simulation, presented by residue index, with alpha helices shown in red and beta strands in blue. This figure summarizes the stability, flexibility, and structural composition of the Hmgcr–Withanolide G complex over time.

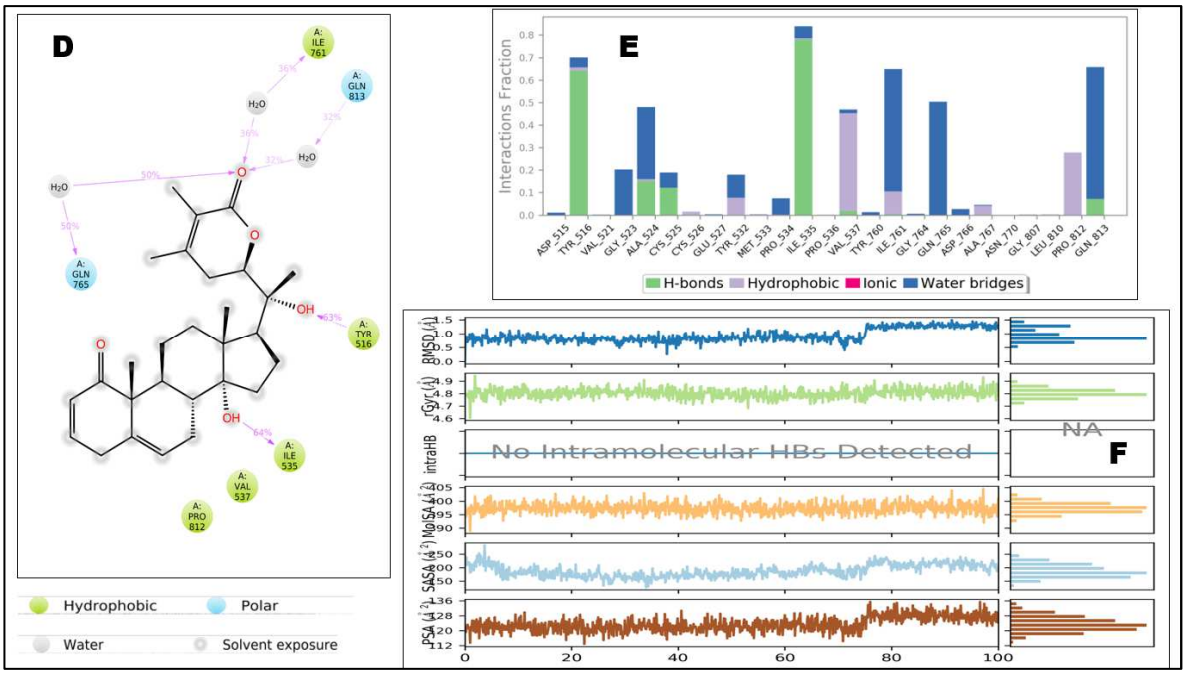

Fig. 4: Molecular dynamics (MD) simulation analysis of the Hmgcr protein (*Mus musculus*) in complex with Withanolide G (continued from Figure 3). (D) Two-dimensional interaction plot summarizing the specific protein–ligand contacts observed during the simulation. (E) Histogram showing the frequency and duration of protein–compound contacts across the simulation, indicating which residues interacted most consistently with Withanolide G. (F) Evaluation of ligand properties, including conformational stability and interaction profiles, assessed at 100 ns of the MD simulation.

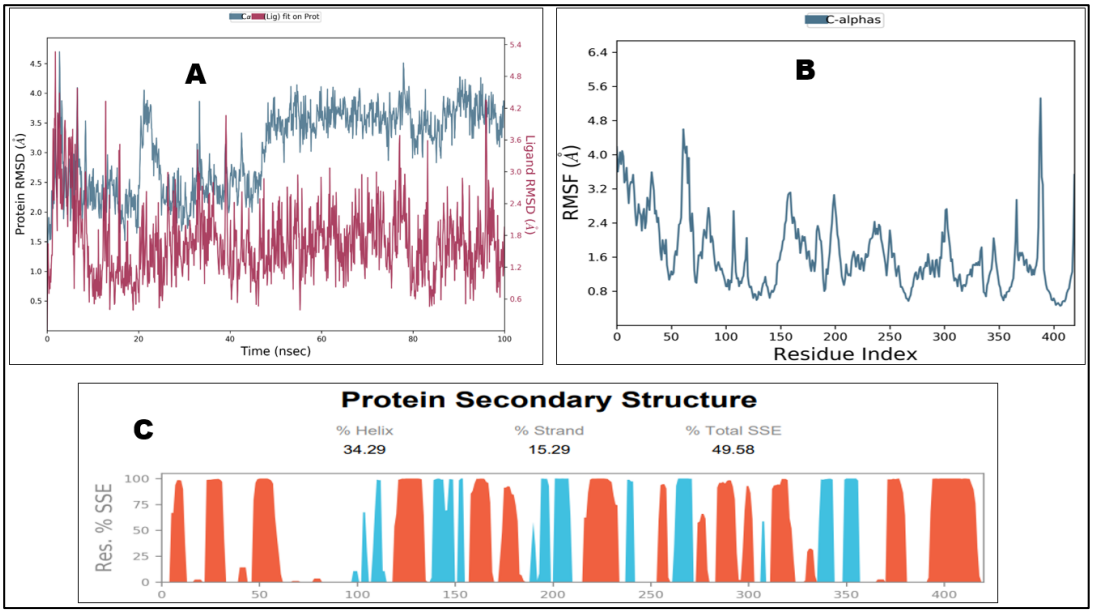

Fig. 5: Molecular dynamics (MD) simulation analysis of the Hmgcr protein (*Mus musculus*) in complex with Coagulin C. (A) Root mean square deviation (RMSD) plot showing the structural stability of the protein (C-alpha atoms, left Y-axis) and the bound ligand (right Y-axis) over the simulation period. (B) Root mean square fluctuation (RMSF) plot depicting the flexibility of individual protein residues during the simulation while complexed with Coagulin C. (C) Distribution of secondary structure elements across the protein during the simulation, organized by residue index, with alpha helices shown in red and beta strands in blue. This figure summarizes the overall stability, residue-level flexibility, and structural composition of the Hmgcr–Coagulin C complex throughout the MD simulation.

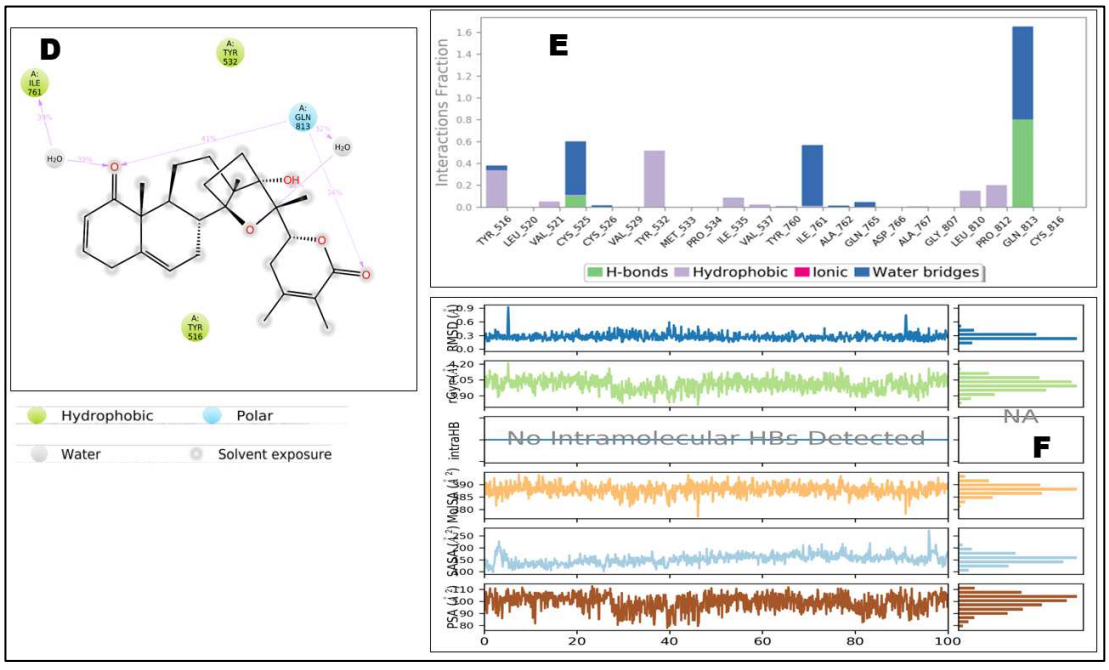

Fig. 6: Molecular dynamics (MD) simulation analysis of the Hmgcr protein (*Mus musculus*) in complex with Coagulin C (continued from Figure 5). (D) Two-dimensional interaction plot summarizing the specific protein–ligand contacts observed during the simulation. (E) Histogram showing the frequency and persistence of protein–Coagulin C contacts throughout the simulation, indicating which residues interacted most consistently. (F) Assessment of ligand properties, including conformational stability and interaction behavior, evaluated at the 100 ns mark of the MD simulation. Together, these panels provide a detailed view of how Coagulin C engaged with Hmgcr over time, highlighting stable contacts and ligand behavior within the binding site.

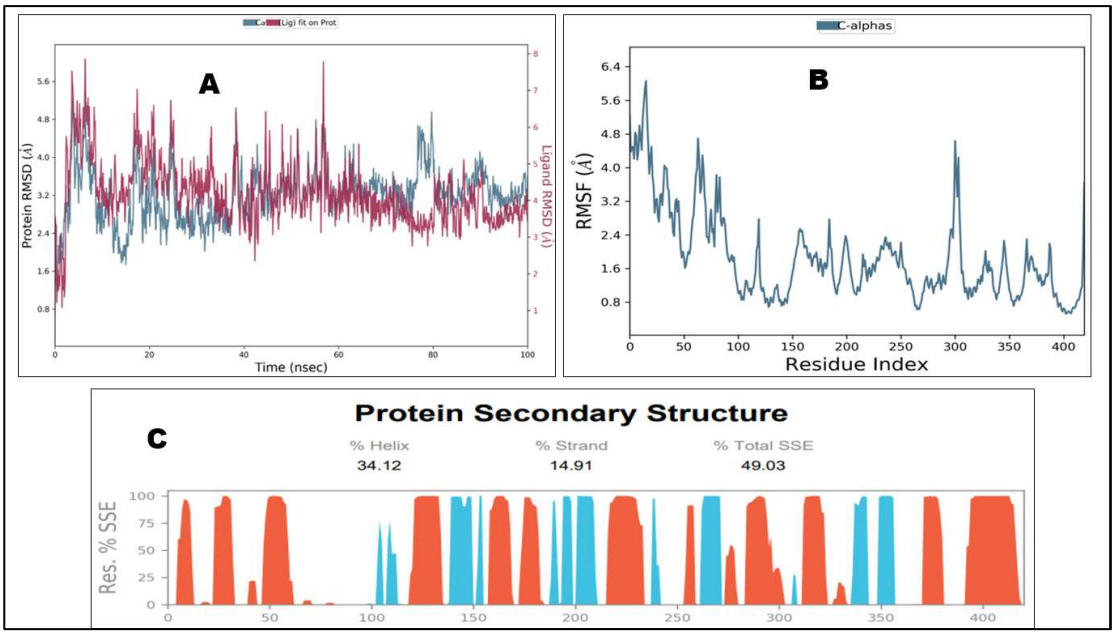

Fig. 7: Molecular dynamics (MD) simulation analysis of the Hmgcr protein (*Mus musculus*) in complex with Withanolide E. (A) Root mean square deviation (RMSD) plot showing the structural stability of the protein (C-alpha atoms, left Y-axis) and the bound ligand (right Y-axis) throughout the simulation period. (B) Root mean square fluctuation (RMSF) plot displaying the flexibility of individual protein residues during the simulation while complexed with Withanolide E. (C) Distribution of secondary structure elements across the protein during the simulation, organized by residue index, with alpha helices shown in red and beta strands in blue. This figure summarizes the stability, residue-level flexibility, and structural composition of the Hmgcr–Withanolide E complex over the course of the MD simulation.

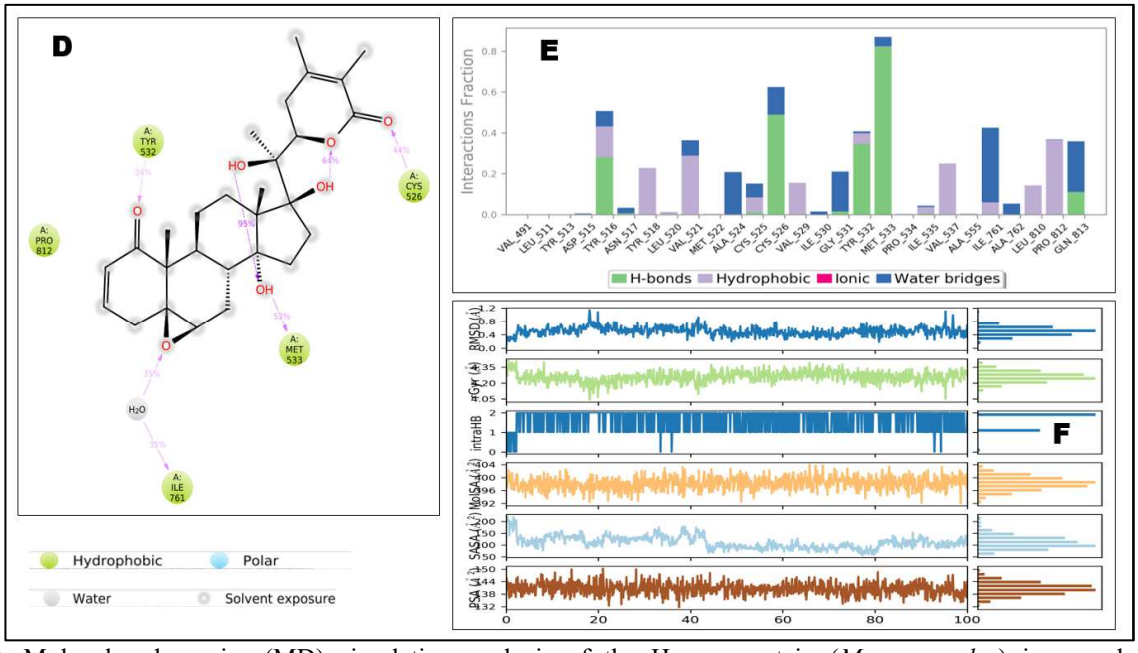

Fig. 8: Molecular dynamics (MD) simulation analysis of the Hmgcr protein (*Mus musculus*) in complex with Withanolide E (continued from Figure 7). (D) Two-dimensional interaction plot showing the specific protein–ligand contacts observed during the simulation. (E) Histogram summarizing the frequency and persistence of protein–Withanolide E contacts across the simulation, highlighting residues that interacted most consistently. (F) Evaluation of ligand properties, including conformational stability and interaction behavior, measured at the 100 ns mark of the MD simulation. Together, these panels provide a detailed overview of how Withanolide E engaged with Hmgcr over time, highlighting key interactions and the stability of the ligand within the binding pocket.

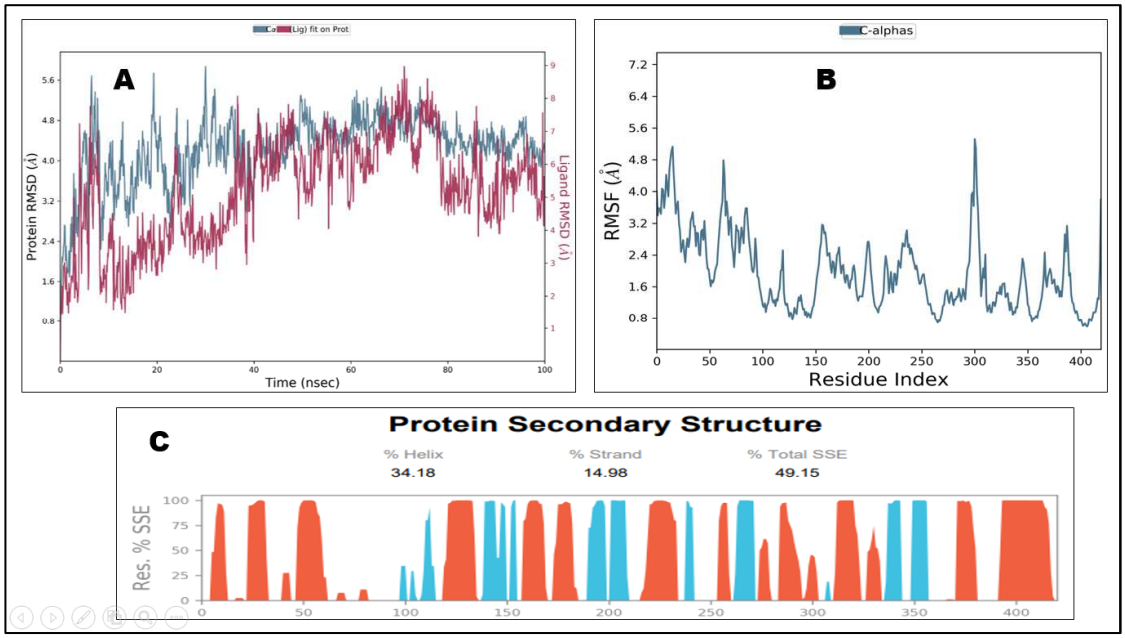

Fig. 9: Molecular dynamics (MD) simulation analysis of the Hmgcr protein (*Mus musculus*) in complex with Withanolide M. (A) Root mean square deviation (RMSD) plot showing the structural stability of the protein (C-alpha atoms, left Y-axis) and the bound ligand (right Y-axis) over the course of the simulation. (B) Root mean square fluctuation (RMSF) plot illustrating the flexibility of individual protein residues while complexed with Withanolide M during the simulation. (C) Distribution of secondary structure elements across the protein throughout the simulation, shown by residue index, with alpha helices in red and beta strands in blue. This figure summarizes the overall stability, residue-level flexibility, and secondary structure behavior of the Hmgcr–Withanolide M complex during MD simulation.

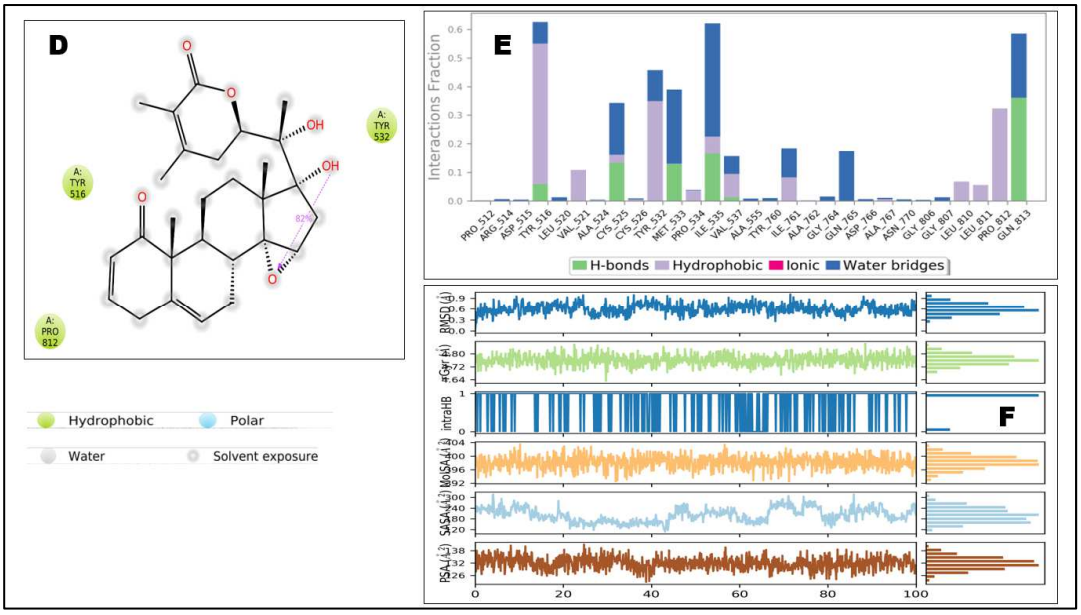

Fig. 10: Molecular dynamics (MD) simulation analysis of the Hmgcr protein (*Mus musculus*) in complex with Withanolide M (continued from Figure 9). (D) Two-dimensional interaction plot summarizing the specific protein–ligand contacts observed during the simulation. (E) Histogram showing the frequency and persistence of protein–Withanolide M contacts across the simulation, identifying residues that consistently interacted with the ligand. (F) Analysis of ligand properties, including conformational stability and interaction behavior, measured at the 100 ns point of the MD simulation. Together, these panels provide a detailed view of how Withanolide M engaged with Hmgcr over time, highlighting key interactions and the stability of the ligand within the binding pocket.

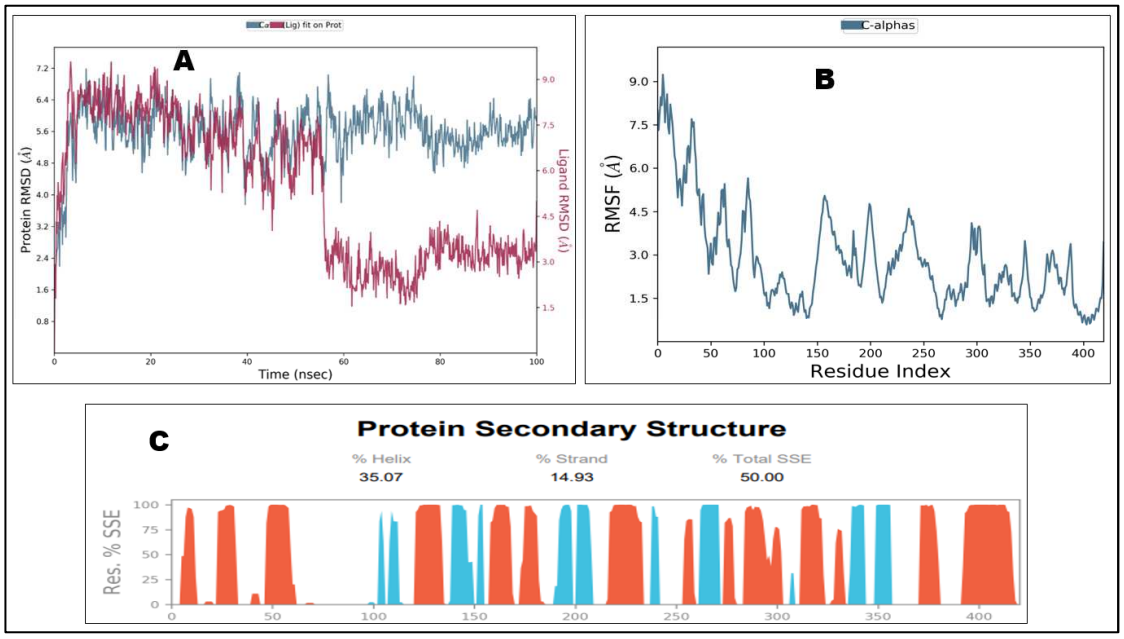

Fig. 11: Molecular dynamics (MD) simulation analysis of the Hmgcr protein (*Mus musculus*) in complex with Coagulanolide. (A) Root mean square deviation (RMSD) plot showing the structural stability of the protein (C-alpha atoms, left Y-axis) and the bound ligand (right Y-axis) throughout the simulation period. (B) Root mean square fluctuation (RMSF) plot illustrating the flexibility of individual protein residues during the simulation while bound to Coagulanolide. (C) Distribution of secondary structure elements across the protein during the simulation, organized by residue index, with alpha helices shown in red and beta strands in blue. This figure summarizes the stability, residue-level flexibility, and secondary structure patterns of the Hmgcr–Coagulanolide complex over the MD simulation period.

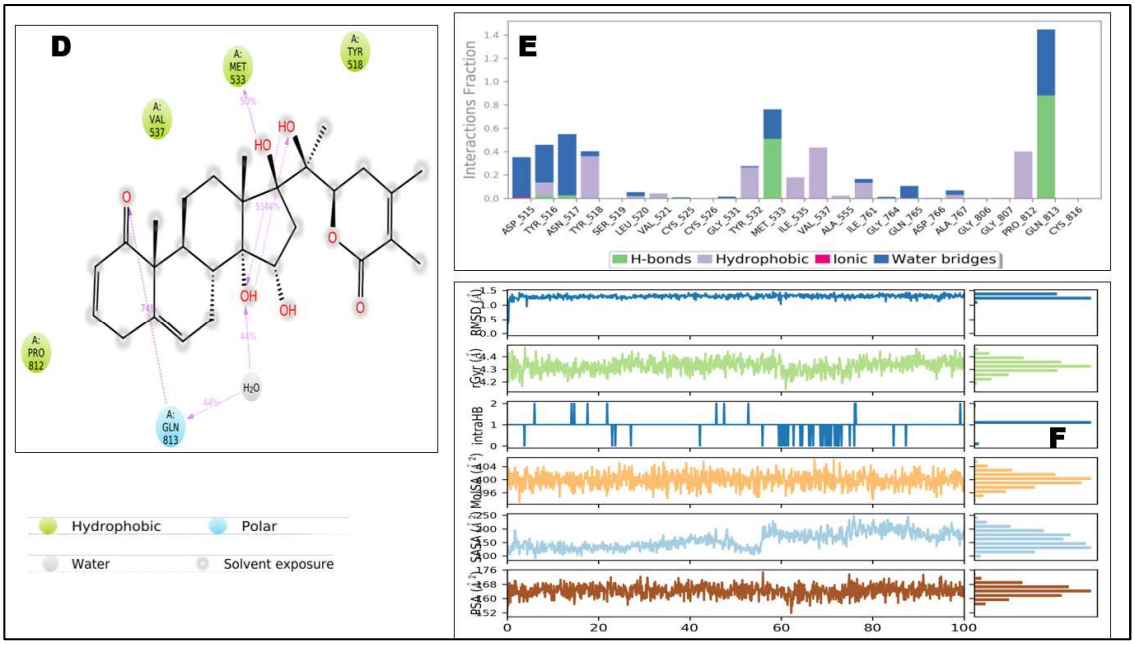

Fig. 12: Molecular dynamics (MD) simulation analysis of the Hmgcr protein (*Mus musculus*) in complex with Coagulanolide (continued from Figure 11). (D) Two-dimensional interaction plot summarizing the specific protein–ligand contacts observed during the simulation. (E) Histogram depicting the frequency and persistence of protein–Coagulanolide contacts throughout the simulation, identifying residues that consistently interacted with the ligand. (F) Evaluation of ligand properties, including conformational stability and interaction behavior, measured at the 100 ns point of the MD simulation. Together, these panels provide a detailed overview of how Coagulanolide interacted with Hmgcr over time, highlighting stable contacts, ligand behavior, and the overall stability of the complex.

Six well-known cholesterol-lowering drugs, namely simvastatin, rosuvastatin, mevastatin, fluvastatin, atorvastatin, and cerivastatin, were retrieved from the compound database, along with their precise 3D chemical structures (Kim *et al*., 2021). Bioactive compounds derived from Withania coagulans represent a promising avenue for discovering alternative therapies. *Withania coagulans*, a plant rich in withanolides, exhibits significant pharmacological potential, particularly in managing metabolic disorders (Khan *et al*., 2021; Sinoriya *et al*., 2024; Tahir *et al*., 2024). The conversion of these compounds into the PDB format ensured compatibility with molecular docking and dynamics simulations, facilitating a detailed interaction analysis with the target protein.

The Lipinski (Pfizer) Rule of Five, a widely recognized standard for evaluating drug-likeness, was used to assess the pharmacokinetic properties of these compounds (Shultz, 2019; Singh and Singh, 2024). The Pfizer Rule of Five, which considers physicochemical properties such as molecular weight and lipophilicity, was applied to the curated compounds, revealing challenges in balancing biological activity with pharmacokinetic compatibility (Singh and Singh, 2024).

ADMET analysis of bioactive compounds in *Withania coagulans* provided insights into the pharmacokinetic and drug-like profiles of various compounds derived from this medicinal plant (Daina *et al*., 2017). The key parameters analyzed included gastrointestinal (GI) absorption, blood-brain barrier (BBB) permeability, P-glycoprotein (P-gp) substrate status, cytochrome P450 enzyme inhibition, log Kp values, bioavailability scores, and synthetic accessibility. Similarly, the bioavailability score of 0.55 reported by SwissADME is an empirical estimate intended for early screening and not a direct measurement of the actual bioavailability *in vivo* (Ferreira and Andricopulo, 2019).

The inhibition of CYP enzymes is a crucial factor in drug-drug interactions (Zhao *et al*., 2021). Limited CYP inhibition suggests a lower risk of drug-drug interactions, making these compounds potentially safer in polypharmacy settings. The lower log Kp values observed for compounds such as 3-HDH-Withanolide F and Withanolide M suggest limited transdermal absorption, which may be beneficial in minimizing systemic exposure during topical application. Therefore, while these findings indicate that the selected compounds meet several criteria consistent with oral drug-like properties, experimental validation is required to confirm their true pharmacokinetic behavior (Daina *et al*., 2017).

Synthetic accessibility scores (6.13 to 6.90) indicated varying levels of synthetic complexity. Higher scores reflect greater structural complexity of natural products, implying challenges in large-scale synthesis and highlighting their potential for unique bioactivity. Therefore, the *in vitro* derivation of synthetic analogs from the main structural skeleton of these compounds derived from *Withania coagulans* would be a valuable addition to the field of drug design and discovery. The ADMET profile of these compounds indicated that *Withania coagulans* contains a range of bioactive compounds with high oral absorption potential and low CNS permeability (Daina *et al*., 2017). The limited inhibition of CYP450 enzymes by most compounds further supports their potential for safe integration into therapeutic regimens, especially in cases where drug-drug interactions are a concern. However, the P-gp substrate status of most compounds may require further investigation to understand its impact on efficacy and resistance, particularly in cells that express high levels of P-gp. Given the moderate synthetic accessibility scores, future studies should focus on optimizing the synthetic routes or extraction methods to make these bioactive compounds more readily available for pharmacological studies and potential therapeutic applications (Ferreira and Andricopulo, 2019).

iGEMDOCK virtual screening identified bioactive compounds from *Withania coagulans* that may inhibit HMG-CoA reductase. It uses a fitness score based on van der Waals, hydrogen bonding, and electrostatic contributions, which were converted into approximate binding energies (ΔG) for comparison with other docking platforms, ensuring consistent interpretation across different methods. Hydrogen bonds play a key role in stabilizing protein-ligand complexes (Bulusu and Desiraju, 2020). The top five compounds (Withaferin A, Withanolide M, Withanolide Q, Ajugin E and Withanolide N) showed consistent binding-site interactions and favorable binding energies. Compounds with higher fitness scores and favorable ΔG values, such as Withaferin A and Withanolide M, exhibited strong interactions with critical residues in the binding pocket. Hydrogen bonds and hydrophobic interactions contribute to specificity and stability, suggesting their potential as effective inhibitors (Bulusu and Desiraju, 2020; Patil *et al*., 2010). Residues such as GLY655 and MET654 were frequently involved in interactions, emphasizing their importance as target sites for designing optimized derivatives of the inhibitors. The repeated engagement of these residues by diverse compounds highlights their role in maintaining ligand stability at the binding site. The strong binding affinities and interaction profiles of these compounds support their use in cholesterol-lowering therapies (Li *et al*., 2019). Withaferin A and Withanolide M, in particular, demonstrated robust profiles, making them promising candidates for further pharmacological evaluation.

The diversity of interactions observed across different compounds provides a foundation for developing derivatives with enhanced activity and specificity (Frye *et al*., 2021). Targeting conserved residues in HMG-CoA

reductase may enhance the efficacy of novel cholesterol-lowering agents (Gunasekaran and Shukor, 2020). Further experimental validation, including *in vitro* and *in vivo* studies, is required to confirm the efficacy and safety of these compounds. Computational analyses, such as molecular dynamics simulations, can offer additional insights into the stability and conformational dynamics of the protein-ligand complexes. These findings highlight the therapeutic potential of these compounds, particularly Withaferin A and Withanolide M, in the management of cholesterol levels. These findings provide a basis for further exploration of natural alternatives for cholesterol-lowering treatments.

In this study, we performed an integrated computational docking and molecular mechanics analysis to evaluate the interactions of Hmgcr protein with both standardized drugs for hypercholesterolemia management and bioactive compounds derived from *Withania coagulans*. This approach provided insights into the predicted binding affinities, interaction dynamics, and energy profiles of these molecules with the target enzyme.

Docking analysis of the Hmgcr protein with selected standardized statins (hypercholesterolemia drugs) showed high binding affinity. Among the tested drugs, simvastatin, atorvastatin, and mevastatin emerged as the top-performing candidates, with docking scores of -7.36, -7.11, and -6.78 kcal/mol, respectively, indicating a strong interaction with the protein (Li *et al*., 2019). The 2D analysis showed that key residues involved in molecular interactions included TYR516, MET533, ILE761, and GLN813. These residues were consistently involved in hydrogen bonding and non-covalent interactions critical for stabilizing the protein–ligand complex (Bulusu and Desiraju, 2020; Patil *et al*., 2010).

To refine these predictions, near-native binding poses were rescored using MM/PB(GB)-SA computations (Wang *et al*., 2019). This additional step improved the accuracy of the binding energy estimations and allowed energy decomposition to reveal the contribution of individual residues to the overall interaction (Wang *et al*., 2019). Heatmap analysis highlighted the top 30 residues contributing to binding across both drug and natural compound complexes in the present study.

A comparative evaluation of standardized drugs and *Withania coagulans* compounds highlighted the better binding affinities of the bioactive compounds from *Withania coagulans*. The compounds not only exhibited higher docking scores but also demonstrated more favorable energetic contributions, as indicated by the MM/PB(GB)-SA analyses (Wang *et al*., 2019). This suggests their potential as natural alternatives or complements to existing hypercholesterolemic drugs.

These findings demonstrate the effectiveness of standardized drugs in binding to Hmgcr and highlight the potential of bioactive compounds from *Withania coagulans* as promising candidates for the management of hypercholesterolemia. Similar *in silico* investigations of natural products have reported comparable trends. For example, several flavonoids showed strong predicted binding affinities to HMG-CoA reductase, in some cases approaching or exceeding that of the native inhibitor, rosuvastatin (−8.5 kcal/mol). Compounds such as rutin (−9.2 kcal/mol) and quercetin (−8.2 kcal/mol) demonstrated particularly favorable interactions (Saputra and Arjita, 2024). These findings suggest that selected flavonoids may act as promising natural candidates for antihyperlipidemic therapy, overlapping with the values observed for withanolides such as Withaferin A and Withanolide M. Similar to our findings, these compounds target key catalytic residues, including TYR516 and MET533, suggesting a conserved binding mechanism among structurally diverse natural molecules.

Deviations are also noteworthy. Some of these studies identified flavonoids with stronger hydrogen bonding but weaker hydrophobic contributions than the steroidal lactones from *Withania coagulans*. In our analysis, withanolides combined stable hydrophobic interactions with conserved hydrogen bonds, potentially offering more balanced binding energetics. These comparisons suggest that while multiple natural compound classes can effectively engage HMG-CoA reductase, the interaction profiles vary depending on the structural scaffolds, which may influence pharmacological properties such as potency and selectivity. The strong binding affinities, favorable energetic profiles, and involvement of critical residues suggest that these compounds could serve as natural alternatives or complementary therapies to traditional statins (Li *et al*., 2019; Patil *et al*., 2010; Wang *et al*., 2019, 2022). Further *in vitro* and *in vivo* studies are required to validate these computational predictions and explore their therapeutic potential.

The top five docked complexes of the Hmgcr protein with *Withania coagulans* bioactive compounds (Withanolide G, Coagulin C, Withanolide E, Withanolide M and Coagulanolide) were subjected to 100 ns molecular dynamics (MD) simulations to evaluate their stability and interaction dynamics (Bera and Payghan, 2019; Malik *et al*., 2023). The simulations revealed key insights into the structural and energetic stabilities of these protein-ligand complexes (Bera and Payghan, 2019).

Throughout the simulations, each ligand maintained its binding pose with minimal deviation and favorable interaction energies, reflecting stable engagement with the target protein. Molecular dynamics simulations confirmed the stable binding of *Withania coagulans* compounds to the Hmgcr protein, with Withanolide G and Coagulin C emerging as promising candidates (Liu *et al*., 2018). Their high stability, minimal residue fluctuations, and robust interaction profiles suggest a strong therapeutic potential

for managing hypercholesterolemia (Bera and Payghan, 2019; Gunasekaran and Shukor, 2020; Liu *et al*., 2018). These findings provide a solid foundation for further experimental validation and pave the way for the development of natural alternatives or adjunctive therapies to complement conventional statin therapy.

Taken together, these molecular dynamics results confirm that *Withania coagulans* compounds form stable complexes with Hmgcr, with Withanolide G and Coagulin C being the most promising candidates. Their consistent stability, low residue fluctuations, and strong interaction networks support their potential for further development as natural therapies for hypercholesterolemia, alongside or as alternatives to conventional statins.

Limitations

Following are some limitations of this study,

1. The study relies on computational predictions and molecular dynamics but does not validate the results experimentally or confirm biochemical inhibition or safety profiles in biological systems.
2. The homology model of *Mus musculus* HMG-CoA reductase, although carefully built and validated, is still a 3-dimensional model, not an experimentally determined structure, and slight variations may affect binding predictions.
3. The study utilized various docking and scoring strategies to verify the findings; however, *in vitro* or *in vivo* studies are crucial for determining the potency, selectivity, and pharmacological relevance of the compounds.

CONCLUSION

The findings suggest that the selected natural compounds exhibit promising inhibitory activity against Hmgcr, making them potential candidates for further experimental validation and drug development. This study underscores the utility of computational drug discovery in identifying novel therapeutic leads that target cholesterol-lowering proteins implicated in hypercholesterolemia.

Acknowledgment

Not applicable

Authors' contributions

MBA: Conceptualization, Data curation, Formal Analysis, Investigation, Methodology, Project administration, Supervision, Validation, Writing–original draft, Writing–review and editing. FK: Data curation, Formal Analysis, Investigation, Methodology, Software, Validation, Writing–original draft. UA: Formal Analysis, Resources, Methodology, Validation, Visualization, Writing–original draft. FH: Formal Analysis, Resources, Validation, Visualization, Writing–original draft. SAS: Formal Analysis, Resources, Validation, Data curation, Writing–original draft, Writing–review and editing. SAQ: Formal Analysis, Resources, Writing–review and editing, Project administration. SDHA: Formal Analysis, Resources, Writing–original draft, Validation.

Funding

The author(s) received no specific funding for this work.

Data availability statement

All relevant data are within the manuscript and its Supporting Information files.

Ethical approval

Not applicable.

Conflict of interest

The authors declare that they have no conflict of interests.

REFERENCES

Ahangari N, Ghayour Mobarhan M, Sahebkar A and Pasdar A (2018). Molecular aspects of hypercholesterolemia treatment: Current perspectives and hopes. *Ann. Med.,* **50**: 303–311.

Azmi MB, Khan F, Asif U, Khurshid B, Wadood A, Qureshi SA, Ahmed SDH, Mudassir HA, Sheikh SI and Feroz N (2023). *In silico* characterization of *Withania coagulans* bioactive compounds as potential inhibitors of hydroxymethylglutaryl (HMG-CoA) reductase of Mus musculus. *ACS Omega*, **8**: 5057–5071.

Bera I and Payghan PV (2019). Use of molecular dynamics simulations in structure-based drug discovery. *Curr. Pharm. Des.,* **25**: 3339–3349.

Björkegren JLM and Lusis AJ (2022). Atherosclerosis: Recent developments. *Cell,* **185**: 1630–1645.

Brown AJ, Coates HW and Sharpe LJ (2021). Cholesterol synthesis. In: Biochemistry of Lipids, Lipoproteins and Membranes. *Elsevier*, pp. 317–355.

Bulusu G and Desiraju GR (2020). Strong and weak hydrogen bonds in protein–ligand recognition. *J. Indian Inst. Sci.,* **100**: 31–41.

Carmena R and Betteridge DJ (2019). Diabetogenic action of statins: Mechanisms. *Curr. Atheroscler. Rep.,* **21**: 23.

Chen L, Fan Z, Chang J, Yang R, Hou H, Guo H, Zhang Y, Yang T, Zhou C, Sui Q, Chen Z, Zheng C, Hao X, Zhang K, Cui R, Zhang Z, Ma H, Ding Y, Zhang N, Lu X, Luo X, Jiang H, Zhang S and Zheng M (2023). Sequence-based drug design as a concept in computational drug design. *Nat. Commun.,* **14**: 4217.

Chen L, Ma MY, Sun M, Jiang LY, Zhao XT, Fang XX, Man Lam S, Shui GH, Luo J, Shi XJ and Song BL (2019). Endogenous sterol intermediates of the mevalonate pathway regulate HMGCR degradation and SREBP-2 processing. *J. Lipid Res.,* **60**: 1765–1775.

Daina A, Michielin O and Zoete V (2017). SwissADME: A free web tool to evaluate pharmacokinetics, drug-likeness and medicinal chemistry friendliness of small molecules. *Sci. Rep.,* **7**: 42717.

Dicken W, Mehta A, Karagiannis A, Jain V, Vavuranakis M, Sperling L and Cassimatis D (2022). Statin associated muscle symptoms: An update and review. *Prog. Cardiovasc. Dis.,* **75**: 40–48.

Ferreira LLG and Andricopulo AD (2019). ADMET modeling approaches in drug discovery. *Drug Discov. Today,* **24**: 1157–1165.

Frye L, Bhat S, Akinsanya K and Abel R (2021). From computer-aided drug discovery to computer-driven drug discovery. *Drug Discov. Today: Technol.,* **39**: 111–117.

Guex N, Peitsch MC and Schwede T (2009). Automated comparative protein structure modeling with SWISS-MODEL and Swiss-PdbViewer: A historical perspective. *Electrophoresis,* **30**: 100–113.

Gunasekaran B and Shukor MY (2020). HMG-CoA Reductase as target for drug development. In: Labrou NE (Ed.), Targeting Enzymes for Pharmaceutical Development. *Methods Mol. Biol.,* Springer, New York, pp. 245–250.

Hsu KC, Chen YF, Lin SR and Yang JM (2011). iGEMDOCK: A graphical environment for enhancing GEMDOCK using pharmacological interactions and post-screening analysis. *BMC Bioinformatics,* **12**: S33.

Jebari-Benslaiman S, Galicia-García U, Larrea-Sebal A, Olaetxea JR, Alloza I, Vandenbroeck K, Benito-Vicente A and Martín C (2022). Pathophysiology of atherosclerosis. *Int. J. Mol. Sci.,* **23**: 3346.

Khan MI, Maqsood M, Saeed RA, Alam A, Sahar A, Kieliszek M, Miecznikowski A, Muzammil HS and Aadil RM (2021). Phytochemistry, food application and therapeutic potential of the medicinal plant Withania coagulans: A review. *Molecules,* **26**: 6881.

Kim S, Chen J, Cheng T, Gindulyte A, He J, He S, Li Q, Shoemaker BA, Thiessen PA, Yu B, Zaslavsky L, Zhang J and Bolton EE (2021). PubChem in 2021: New data content and improved web interfaces. *Nucleic Acids Res.,* **49**: D1388–D1395.

Li J, Fu A and Zhang L (2019). An overview of scoring functions used for protein–ligand interactions in molecular docking. *Interdiscip. Sci.,* **11**: 320–328.

Liu X, Shi D, Zhou S, Liu H, Liu H, Yao X (2018). Molecular dynamics simulations and novel drug discovery. *Expert Opin. Drug Discov.,* **13**: 23–37.

Malik A, Iqbal MN, Ashraf S, Khan MS, Shahzadi S, Shafique MF, Sajid Z, Sajid M and Sehgal SA (2023). In silico elucidation of potential drug targets against oxygenase domain of human eNOS dysfunction. *PLOS ONE,* **18**: e0284993.

Nwozo OS, Effiong EM, Aja PM and Awuchi CG (2023). Antioxidant, phytochemical and therapeutic properties of medicinal plants: A review. *Int. J. Food Prop.,* **26**: 359–388.

Patil R, Das S, Stanley A, Yadav L, Sudhakar A and Varma AK (2010). Optimized hydrophobic interactions and hydrogen bonding at the target–ligand interface lead pathways of drug designing. *Plos ONE,* **5**: e12029.

Pettersen EF, Goddard TD, Huang CC, Meng EC, Couch GS, Croll TI, Morris JH and Ferrin TE (2021). UCSF Chimera X: Structure visualization for researchers, educators and developers. *Protein Sci.,* **30**: 70–82.

Pinal-Fernandez I, Casal-Dominguez M and Mammen AL (2018). Statins: Pros and cons. *Med. Clin. (Barc),* **150**: 398–402.

Prasad K and Mishra M (2022). Mechanism of hypercholesterolemia-induced atherosclerosis. *Rev. Cardiovasc. Med.,* **23**: 212.

Saputra IPBA and Arjita IPD (2024). The potential of flavonoid derivative compounds as inhibitors of the HMG-CoA reductase enzyme for candidate hypercholesterolemia drugs. *J. Penelit. Pendidik. IPA,* **10**: 2286–2293.

Sayers EW, Beck J, Bolton EE, Bourexis D, Brister JR, Canese K, Comeau DC, Funk K, Kim S, Klimke W, Marchler-Bauer A, Landrum M, Lathrop S, Lu Z, Madden TL, O'Leary N, Phan L, Rangwala SH, Schneider VA, Skripchenko Y, Wang J, Ye J, Trawick BW, Pruitt KD and Sherry ST (2021). Database resources of the National Center for Biotechnology Information. *Nucleic Acids Res.,* **49**: D10–D17.

Shultz MD (2019). Two decades under the influence of the Rule of Five and the changing properties of approved oral drugs. *J. Med. Chem.,* **62**: 1701–1714.

Singh R and Singh K (2024). Lipinski's Rule of Five. In: Singh R, Kumar A and Singh K (Eds.), *2-Deoxy-D-Glucose: Chemistry and Biology*. *Bentham Science Publishers*, pp. 242–246.

Sinoriya P, Kaushik R, Sinoria A and Gaur PK (2024). Comprehensive review on *Withania coagulans* Dunal: Unveiling pharmacognosy, phytochemistry and pharmacological potentials. *Pharmacogn. Rev.,* **18**: 47–59.

Tahir T, Javed M, Ahmed W, Iahtisham-Ul-Haq, Wang Q, Khan MI and Huang Z (2024). Therapeutic uses and pharmacological properties of the traditional South Asian medicinal plant *Withania coagulans*. *J. Herb. Med.,* **47**: 100926.

Wang E, Sun H, Wang J, Wang Z, Liu H, Zhang JZH and Hou T (2019). End-point binding free energy calculation with MM/PBSA and MM/GBSA: Strategies and applications in drug design. *Chem. Rev.,* **119**: 9478–9508.

Wang Z, Pan H, Sun H, Kang Y, Liu H, Cao D and Hou T (2022). fastDRH: A webserver to predict and analyze protein–ligand complexes based on molecular docking and MM/PB(GB)SA computation. *Brief. Bioinform.,* **23**: bbac201.

Waterhouse A, Bertoni M, Bienert S, Studer G, Tauriello G, Gumienny R, Heer FT, de Beer TAP, Rempfer C, Bordoli L, Lepore R and Schwede T (2018). SWISS-MODEL: Homology modelling of protein structures and complexes. *Nucleic Acids Res.,* **46**: W296–W303.

Webb B and Sali A (2021). Protein structure modeling with MODELLER. In: Chen YW and Yiu CPB (Eds.),

Structural Genomics. *Methods Mol. Biol.,* Springer, New York, pp. 239–255.

Zhao M, Ma J, Li M, Zhang Y, Jiang B, Zhao X, Huai C, Shen L, Zhang N, He L and Qin S (2021). Cytochrome P450 enzymes and drug metabolism in humans. *Int. J. Mol. Sci.,* **22**: 12808.

Zheng J, Wang J, Zhang Y, Xia J, Guo H, Hu H, Shan P and Li T (2022). The global burden of diseases attributed to high low-density lipoprotein cholesterol from 1990 to 2019. *Front. Public Health,* **10**: 891929.